Oil & Natural Gas Technology

DOE Award No.: DE-NT0005669

Final Scientific/Technical Report

October 1 2008 to June 30 2011

Heat Flow and Gas Hydrates on the Continental Margin of India: Building on Results from NGHP Expedition 01

Submitted by:
College of Oceanic and Atmospheric Science
Oregon State University
Corvallis, OR 97331-5503

Principal Investigator: Anne Trehu
Graduate Research Assistant: Peter Kannberg

Prepared for:
United States Department of Energy
National Energy Technology Laboratory

November 15, 2012

Office of Fossil Energy

Abstract

The Indian National Gas Hydrate Program (NGHP) Expedition 01 presented the unique opportunity to constrain regional heat flow derived from seismic observations by using drilling data in three regions on the continental margin of India. The seismic bottom simulating reflection (BSR) is a well-documented feature in hydrate bearing sediments, and can serve as a proxy for apparent heat flow if data are available to estimate acoustic velocity and density in water and sediments, thermal conductivity, and seafloor temperature. Direct observations of temperature at depth and physical properties of the sediment obtained from drilling can be used to calibrate the seismic observations, decreasing the uncertainty of the seismically-derived estimates. Anomalies in apparent heat flow can result from a variety of sources, including sedimentation, erosion, topographic refraction and fluid flow. We constructed apparent heat flow maps for portions of the Krishna-Godavari (K-G) basin, the Mahanadi basin, and the Andaman basin and modeled anomalies using 1-D conductive thermal models.

Apparent heat flow values in the Krishna-Godavari (K-G) basin and Mahanadi basin are generally 0.035 to 0.055 watts per square meter (W/m^2). The borehole data show an increase in apparent heat flow as water depth increases from 900 to 1500 m. In the SW part of the seismic grid, 1D modeling of the effect of sedimentation on heat flow shows that ~50% of the observed increase in apparent heat flow with increasing water depth can be attributed to trapping of sediments behind a "toe-thrust" ridge that is forming along the seaward edge of a thick, rapidly accumulating deltaic sediment pile. The remainder of the anomaly can be explained either by a decrease in thermal conductivity of the sediments filling the slope basin or by lateral advection of heat through fluid flow along stratigraphic horizons within the basin and through flexural faults in the crest of the anticline. Such flow probably plays a role in bringing methane into the ridge formed by the toe-thrust. Because of the small anomaly due to this process and the uncertainty in thermal conductivity, we did not model this process explicitly. In the NE part of the K-G basin seismic grid, a number of local heat flow lows and highs are observed, which can be attributed to topographic refraction and to local fluid flow along faults, respectively. No regional anomaly can be resolved. Because of lack of continuity between the K-G basin sites within the seismic grid and those ~70 km to the NE in water depths of 1200 to 1500 m, we do not speculate on the reason for higher heat flow at these depths. The Mahanadi basin results, while limited in geographic extent, are similar to those for the K-G basin.

The Andaman basin exhibits much lower apparent heat flow values, ranging from 0.015 to 0.025 W/m^2. Heat flow here also appears to increase with increasing water depth. The very low heat flow here is among the lowest heat flow observed anywhere and gives rise to a very thick hydrate stability zone in the sediments. Through 1D models of sedimentation (with extremely high sedimentation rates as a proxy for tectonic

thickening), we concluded that the very low heat flow can probably be attributed to the combined effects of high sedimentation rate, low thermal conductivity, tectonic thickening of sediments and the cooling effect of a subducting plate in a subduction zone forearc. Like for the K-G basin, much of the local variability can be attributed to topography. The regional increase in heat flow with water depth remains unexplained because the seismic grid available to us did not extend far enough to define the local tectonic setting of the slope basin controlling this observational pattern.

The results are compared to results from other margins, both active and passive. While an increase in apparent heat flow with increasing water depth is widely observed, it is likely a result of different processes in different places. The very low heat flow due to sedimentation and tectonics in the Andaman basin is at the low end of global observations from forearc basins, possibly because of unusually high regional sedimentation rates and a high rate of tectonic deformation.

In addition to providing an opportunity to follow up on preliminary results from NGHP-01, which was partially funded by DOE to increase understanding of submarine gas hydrates, a primary objective of this project was to provide training for a graduate student who had participated in the data acquisition as a technician. Our approach was to start with very simple analytic models to develop intuition about the relative importance of different parameters both as a learning exercise and to evaluate whether a more complex modeling effort could be constrained by the existing data.

Table of Contents

Executive Summary

The Indian National Gas Hydrate Program (NGHP) Expedition 01 presented the unique opportunity to constrain regional heat flow derived from seismic observations by using drilling data in three regions on the continental margin of India. The seismic bottom simulating reflection (BSR) is a well-documented feature in hydrate bearing sediments, and can serve as a proxy for apparent heat flow if data are available to estimate acoustic velocity and density in water and sediments, thermal conductivity, and seafloor temperature. Direct observations of temperature at depth and physical properties of the sediment obtained from drilling can be used to calibrate the seismic observations, decreasing the uncertainty of the seismically-derived estimates. Anomalies in apparent heat flow can result from a variety of sources, including sedimentation, erosion, topographic refraction and fluid flow. We constructed apparent heat flow maps for portions of the Krishna-Godavari (K-G) basin, the Mahanadi basin, and the Andaman basin and modeled anomalies using 1-D conductive thermal models.

Apparent heat flow values in the Krishna-Godavari (K-G) basin and Mahanadi basin are generally 0.035 to 0.055 W/m^2. The borehole data show an increase in apparent heat flow as water depth increases from 900 to 1500 m. In the SW part of the seismic grid, 1D modeling of the effect of sedimentation on heat flow shows that ~50% of the observed increase in apparent heat flow with increasing water depth can be attributed to trapping of sediments behind a "toe-thrust" ridge that is forming along the seaward edge of a thick, rapidly accumulating deltaic sediment pile. The remainder of the anomaly can be explained either by a decrease in thermal conductivity of the sediments filling the slope basin or by lateral advection of heat through fluid flow along stratigraphic horizons within the basin and through flexural faults in the crest of the anticline. Such flow probably plays a role in bringing methane into the ridge formed by the toe-thrust. Because of the small anomaly due to this process and the uncertainty in thermal conductivity, we did not model this process explicitly. In the NE part of the K-G basin seismic grid, a number of local heat flow lows and highs are observed, which can be attributed to topographic refraction and to local fluid flow along faults, respectively. No regional anomaly can be resolved. Because of lack of continuity between the K-G basin sites within the seismic grid and those ~70 km to the NE in water depths of 1200 to 1500 m, we do not speculate on the reason for higher heat flow at these depths. The Mahanadi basin results, while limited in geographic extent, are similar to those for the K-G basin.

The Andaman basin exhibits much lower apparent heat flow values, ranging from 0.015 to 0.025 W/m^2. Heat flow here also appears to increase with increasing water depth. The very low heat flow here is among the lowest heat flow observed anywhere and gives rise to a very thick hydrate stability zone in the sediments. Through 1D models of sedimentation (with extremely high sedimentation rates as a proxy for tectonic

thickening), we concluded that the very low heat flow can probably be attributed to the combined effects of high sedimentation rate, low thermal conductivity, tectonic thickening of sediments and the cooling effect of a subducting plate in a subduction zone forearc. Like for the K-G basin, much of the local variability can be attributed to topography. The regional increase in heat flow with water depth remains unexplained because the seismic grid available to us did not extend far enough to define the local tectonic setting of the slope basin controlling this observational pattern.

The results are compared to results from other margins, both active and passive. While an increase in apparent heat flow with increasing water depth is widely observed, it is likely a result of different processes in different places. The very low heat flow due to sedimentation and tectonics in the Andaman basin is at the low end of global observations from forearc basins, possibly because of unusually high regional sedimentation rates and a high rate of tectonic deformation.

In addition to providing an opportunity to follow up on preliminary results from NGHP-01, which was partially funded by DOE to increase understanding of submarine gas hydrates, a primary objective of this project was to provide training for a graduate student who had participated in the data acquisition as a technician. Our approach was to start with very simple analytic models to develop intuition about the relative importance of different parameters both as a learning exercise and to evaluate whether a more complex modeling effort could be constrained by the existing data.

Introduction

Submarine gas hydrate is a clathrate of water, methane, and sometimes other trace gasses like carbon dioxide and ethane. At high pressures and low temperatures, such as those found on continental margins, gas molecules such as methane can become encompassed by a cage-like structure of water molecules, forming a solid ice-like substance when the amount of gas present is great than its solubility in porewater, which depends on the gas composition and pore water salinity as well as the ambient temperature and pressure.

In many continental margin environments the presence of gas hydrate is indicated by a characteristic seismic reflection commonly referred to as the bottom simulating reflection (BSR), which is a seismic reflection with polarity that is opposite to that of seafloor that cross-cuts reflections of stratigraphic origin (Shipley et al., 1979). The BSR is interpreted to indicate the temperature and pressure boundary at which hydrate forms, resulting in a relatively a high-velocity, possibly hydrate-bearing zone overlying a low-velocity region that contains free gas (e.g. Bangs et al., 1993; Hyndman et al., 1993; Korenaga et al., 1997; Tréhu et al., 1995; 2003; Zwart et al., 1996; Ganguly et al., 2000). If heat transport is dominated by conductive transport, Fourier's law of thermal conduction states that heat flow is the product of the bulk thermal conductivity and the temperature gradient. Where BSRs are present, apparent heat flow can be determined from the BSR depth (Yamano et al., 1982), sediment density and thermal conductivity, pore water and gas chemistry and seafloor temperature. Borehole temperature and physical property measurements can be used to verify whether the thermal gradient is piecewise linear (as expected for a conductive environment) and provide accurate values for converting BSR travel-ties to apparent heat flow, thus extending heat flow constraints from the borehole to the surrounding region and providing new information on tectonic, sedimentary and hydrologic processes that affect heat flow and gas hydrate distribution (e.g. Villinger et al., 2010).

The Indian National Gas Hydrate Program (NGHP) conducted its first gas hydrate drilling expedition from April 28 to August 19, 2006. Pre-cruise seismic surveying efforts reported extensive bottom simulating reflectors in the Krishna-Godavari (K-G) basin, Mahanadi basin, and Andaman Sea (Figure 1A). These initial seismic surveys form the basis of this study. Building upon these surveys, and serving as a calibration tool, are borehole temperature measurements taken aboard the JOIDES Resolution during the 113-day expedition. NGHP thus offers the opportunity to determine heat flow from both methods in same geographic region. Additionally, information from core samples on sedimentation history provides constraints for models to constrain the impact of sedimentary tectonics, deposition rate and erosion on apparent heat flow.

The tectonic settings of the K-G and Andaman basins are shown in Figures 1B and 2A, respectively. The Krishna Godavari (K-G) basin originated with Mesozoic rifting and subsequent formation of an ocean basin and extends across the passive continental margin of southeastern India (Rao, 2001). The continent/ocean boundary is thought to occur near the base of the slope (corresponding to the 3000 m contour on Figure 1B) based on magnetic anomalies (Murthy et al., 1995). Onshore, the basin is covered by alluvial sediments (Gupta, 2006), but indications of rift-related horsts and grabens extend ~50 km from the coastline (Dewangen et al., 2011). The study area is therefore located approximately in the middle of a 250 km wide region of rifted and possibly intruded continental crust, similar to the Atlantic continental margin of the US (e.g. Ruppel et al., 1995). The hydrocarbon potential of this basin motivated NGHP-01 (Collett et al., 2008) as well as many other studies. The tectonic setting of the Mahanadi basin is similar (Figure 1A).

The Andaman basin is a forearc basin located just west of the Andaman Islands in the western Bay of Bengal (Figure 2A). The geologic and tectonic setting of this region has recently been reviewed by Cochran (2010). Subduction along this segment of the Sumatra subduction zone was initiated ~65 Ma and is currently highly oblique. As is common for highly oblique subduction zones, there are few active volcanoes along this segment of the arc, unlike further to the southeast, where there is a vigorous volcanic arc on the island of Sumatra. Instead, the backarc is characterized by strike-slip faulting and possibly backarc extension. Site 17 was located on the eastern flank of a forearc high that emerges above sea level in the Andaman Islands. Seismic reflection profiles show a thick package of sediments with complex folding and faulting in this region (Figure 2B). Site 17 is on a local ridge that has been interpreted to be a fault marking the boundary between the forearc high and the forearc basin to the east. Cochran (2010) speculates that the region between the Eastern Margin Fault and the West Andaman Fault is analogous to the Aleutian forearc basin, which is thought to have formed because of subduction erosion, which thinned the basement crust from below.

Initial analyses of the borehole temperatures conducted during NGHP-01 showed remarkable consistence between the depth to the base of the gas hydrate stability field (BGHS) predicted by seismic observations of the BSR and the BGHS predicted by in situ temperatures recorded in the boreholes (Table 1). These preliminary analyses also indicated that the temperature gradients in the boreholes increased with increasing water depth in the K-G basin (Figure 1C) and that thermal conductivity of the sediments did not vary enough to compensate for this when thermal gradient was converted to heat flow. Finally, the data indicated that the heat flow in the Andaman Sea (Site 17) was very low, even when compared to other forearc basins (Table 1).

For this project we determined regional heat flow patterns in the K-G, Mahanadi and Andaman basins using drilling and seismic data to evaluate whether the apparent heat flow increase with water depth could be interpreted as indicative of large-scale fluid flow,

which could affect the migration of gas through the sediments and consequently control the distribution of gas hydrate. However, conductive modeling of the effects of sedimentation and topographic refraction combined with local stratigraphic and regional tectonic characteristics was adequate to explain most of the heat flow variation.

Heat flow methods

Borehole temperature measurements

Downhole temperature measurements were taken aboard the DV JOIDES Resolution. The APCT-3 and Davis-Villinger Temperature Probe (DVTP) were used to take these measurements (Davis et al., 1997). Both tools employ a thermistor to determine temperature. The APCT-3 is a second-generation temperature tool located within the cutting show of the advanced piston core (APC) (Heesemann et al. 2006). The APC is used to recover shallow, unconsolidated sediment and as such, the APCT-3 is only usable until APC refusal, where the sediment strength becomes too high for the APC to penetrate. The APCT-3 has a narrow, needle-like probe containing the thermistor that extends to near the tip of the APC cutting shoe, where the thermal mass will be smallest. The needle is coated in thermal grease to ensure thermal contact with the surrounding shoe.

At APC refusal, the APC is replaced with the extended core barrel (XCB) and the DVTP is used to take temperature measurements. The APC was occasionally replaced with the XCB before refusal because the fluid circulated to enable drilling with the XCB cools the formation, allowing for greater recovery in hydrate-rich, gaseous sediment (e.g. Tréhu et al. 2004). The DVTP is a long, cone-shaped probe that replaces the XCB in the drill string. The DVTP extends beyond the end of the drill string and is pushed into the undisturbed sediment below. The DVTP is then uncoupled from the drill string so that it will remain undisturbed in the sediment. The DVTP electronics package also has an on-board accelerometer to determine if the tool remained seated during the entire equilibrium time. When deployed, the DVTP replaces the core barrel, requiring a dedicated tool run.

When the probe enters the sediment, a pulse of heat is observed due to friction (Figure 3A). The temperature decay curve from the initial frictional temperature spike is extrapolated to determine the original temperature of the formation. Because the DVTP must penetrate stiffer sediment, it is a larger, more robust tool, but generates a smaller frictional pulse because the tool is slowly pushed 1 to 1.5 m into the formation, rather than shot ~10 m into the formation, as is the case with the APCT-3. Both tools require at least 15 to 20 minutes in the formation to record a temperature decay history that can be robustly extrapolated to the in situ temperature. High seas or unstable formations can cause the tool to uncouple from the sediment, introducing perturbations in the temperature decay curve. The programs that fit the data to a theoretical temperature

decay curve include the theoretical effects of tool geometry and the thermal conductivity and diffusivity of the sediment. The interpreter must use discretion in choosing the parameters as well as the window of data to include in the analysis. Temperature measurements were taken at multiple depths in each hole, establishing the geothermal gradient for each site. Only good quality data were used to derive temperature versus depth profiles in the NGHP-01 boreholes. The entire dataset along with evaluations of data quality and the calculations to determine the best fitting temperature gradient in each borehole can be found in the NGHP-01 Initial Report (Collett et al., 2008). Some examples are given in Figure 3B.

Apparent heat flow from BSR observations

Pre-cruise 2-D seismic surveys were performed to guide site selection and hazard assessment (unpublished cruise prospectus). A subset of these data were provided to us by M. Riedel (Pacific Geoscience Center), including grids of seismic lines in the K-G and Andaman basins and an X-shaped survey comprising three closely-spaced lines in each direction for the Mahanadi basin. These surveys provide an extensive record of the BSR, which is easily recognized by the velocity inversion and cross-cutting relationship with bedding (Figure 4). Swath bathymetry was also available for the K-G basin, and we determined bathymetry from the seismic data for the Andaman and Mahanadi basins. The gas hydrate stability zone (GHSZ) in the vicinity of NGHP-01 Site 17 is shown in Figure 5. In the following paragraphs, we discuss the data we used to determine the parameters entering into this calculation.

BSR depth was calculated from two-way travel times along seismic sections and from P-wave velocity in the ocean and in the sediments. A seawater velocity of 1486 m/s was used based on regional temperature and salinity (Wong and Zhu, 1995). For the K-G and Mahanadi basins, an average sediment P-wave velocity of 1550 m/s was used based on downhole logging data (Figure 6A). A sediment P-wave velocity of 1600 m/s was used in the Andaman basin based on strong constraints from a vertical seismic profile (Figure 6B). While in some cases of low methane flux, the top of the free gas zone may be tens of meters below the GHSZ (Xu and Ruppel, 1999), drilling results confirm that in the K-G, Mahanadi, and Andaman basins, the BSR is coincident with the base of the GHSZ. At all sites, geothermal gradients constructed from downhole temperature tool measurements intersected the GHSZ at depths consistent with the BSR depth (Table 1). Additional indications of hydrate presence overlying free gas, such as decreasing resistivity, velocity, and density, as well as increasing porosity at the depth of the BSR, were present in downhole logging data (Collett et al. 2008). In general, we estimate ~3% uncertainty in the estimate of average velocity between the seafloor and the BSR.

Thermal conductivity is normally measured in core samples by heating the sediment slightly with a needle-like probe; the temperature of the probe is then measured to determine how the heat dissipates through the medium. In hydrate bearing formations,

however, the sediment is usually too disturbed to provide accurate estimates of in situ temperature by this method (Figure 7). As a hydrate-bearing core sample is brought to the surface for shipboard measurements, the hydrate will dissociate, leaving behind the residual water and void spaces, creating 'foamy' sediment with very different physical properties than the in situ sediment. Even when no hydrate is present, gases dissolved in the pore water are often released upon recovery as the solubility decreases, creating small cracks in the sediment that reduce thermal conductivity. While these areas were avoided as much as possible when making shipboard measurements, the thermal conductivities of sediments recovered from the NGHP study areas are lower than thermal conductivities documented at other margins (Grevemeyer and Villinger 2000) and some of the scatter, especially among lower values, may be due to microcracks due to gas exsolution. For this study, we ignored outlying values and assumed a thermal conductivity of 0.95 watts per meter per degree Kelvin (Wm^1K^{-1}) for the K-G basin and 0.90 $Wm^{-1}K^{-1}$ for the Mahanadi and Andaman basins based on the envelope of the data and dominant sediment type (clay). This is a significant source of uncertainty in the heat flow estimates, which we estimate to be ~5%.

To estimate temperature at the BSR, it is also necessary to know the seafloor temperature. Because seafloor temperature varies with water depth and the measurements taken with the temperature tool before it enters the borehole (Figure 3A) can be affected by short-term variations due to tidal and seasonal effects in continental margin water depths, we used data from the World Ocean Atlas 2005 to determine the water column temperature profile at each of the 3 study regions (Figure 8). The temperature at the seafloor at each point was determined from the intersection of the regional water column temperature profile as the seafloor depth determined from swath bathymetry or from the two-way travel (TWT) times to seafloor observed in the seismic data. Seafloor temperatures determined in this way were within ±0.25°C of the temperature measured immediately prior to insertion of the probe into the seafloor. In the Andaman Basin, the seafloor temperature calculated from the World Ocean Atlas fell within 0.05°C of the measured value at NGHP site 17. We estimate that uncertainty in the long-term average seafloor temperature is ~1%.

The India Directorate General of Hydrocarbons processed the seismic lines, which were then provided to us. Kingdom Suites software tools were used to pick BSR and seafloor reflection times. These picks were then gridded and exported for analysis in Matlab. While the seafloor picks encompass the entire study region, the BSR is not present in all places. Where BSRs were absent, multiple techniques were tried to interpolate the gaps. Spline, nearest neighbor, and Kriging interpolation techniques were all tried, but a simple nearest neighbor interpolation technique was able to track the seafloor and BSR most accurately. Blank spots in the BSR maps indicate regions where interpolation was deemed unreliable. While the details of local anomalies are not reliable where large gradients in apparent heat flow occur off of seismic line, the general patterns are well constrained by the data.

In order to calculate BSR temperature, the BSR depth must first be determined from the following equation:

$$BSR_{depth} = V_{sed} \times (BSR_{OWT} - seafloor_{OWT}) + V_{water} \times seafloor_{OWT} \quad \text{(Eq. 1)}$$

where BSR_{depth} is the depth, in meters below sea level, of the seismic BSR, BSR_{OWT} and $seafloor_{OWT}$ are one-way travel times (OWT) to the BSR and seafloor, and V_{sed} and V_{water} are average P-wave velocities of sediment and water in these intervals. BSR depth is then converted to pressure. Although there is some controversy about whether to use lithospheric or hydrostatic pressure (He et al. 2009, Ganguly et al. 2000; Hyndman et al., 1993), most previous studies have found that the inferred temperature at the base of the HSZ better matches the dissociation curve if hydrostatic pressure is assumed (e.g. Martin et al. 2004; Tréhu et al. 1995; Tréhu et al. 2006). We therefore assumed hydrostatic pressure.

In the final step, the temperature at the BSR implied by the calculated BSR was determined from the empirical relationship of Maekawa et al. (1995). A pure methane hydrate and 3.5% saline pore water were used. Porewater measurements during NGHP-01 indicated that porewater salinity at the BSR ranged from 3.0 to 3.5 at all sites (Figure 9; Collett et al., 2008). We estimate an uncertainty of ~1% in apparent heat flow due to assuming a seawater salinity.

Heat flow is calculated from Fourier's 1-D heat flow equation assuming constant thermal gradient and thermal conductivity between the seafloor and the BSR:

$$q = -k\left(\frac{T_{BSR} - T_{seafloor}}{depth_{BSR} - depth_{seafloor}}\right) \quad \text{(Eq. 2)}$$

where q is heat flow in W/m^2, k is thermal conductivity, T_{BSR} and $T_{seafloor}$ are temperature at the BSR and seafloor, and $depth_{BSR}$ and $depth_{seafloor}$ are depth from two-way travel time for the BSR and seafloor. Apparent heat flow values were calculated in this manner for the K-G basin, Mahanadi basin, and Andaman Sea to generate grids with a spacing of 100x100 m. Adding the estimated uncertainty of all the parameters entering into this calculation, we estimate an uncertainty of ~10%, with half coming from uncertainty in the thermal conductivity.

Regional heat flow maps

Krishna-Godavari basin - Geologic Setting

The Krishna Godavari (K-G) basin originated with Mesozoic rifting and subsequent formation of an ocean basin and extends across the passive continental margin of

southeastern India (Rao, 2001). The continent/ocean boundary is thought to occur near the base of the slope based on magnetic anomalies (Murthy et al., 1995). Onshore, the basin is covered by alluvial sediments (Gupta, 2006), but indications of rift-related horsts and grabens extend ~50 km from the coastline (Dewangen et al., 2011). The study area is therefore located approximately in the middle of a 250 km wide region of rifted and possibly intruded continental crust, similar to the Atlantic continental margin of the US (e.g. Ruppel et al., 1995).

Offshore, recent sediment input is dominated by the deltas of the Krishna and Godavari rivers and total sediment thickness may reach up to 8 km (Rao, 2001). The dominant lithology in the sediments sampled during NGHP-01 is clay, with silt as a minor lithology and some authigenic carbonate-rich zones (Collett et al. 2008). Stratigraphic environments across the margin include a wide range of passive margin depositional settings, including delta, shelf-slope apron, deep-sea channels and channel-levee, and deep-water fan deposits (Shankar and Riedel, 2010). In particular, the very rapid sediment flux has lead to a topography on the mid-slope characterized by arcuate ridges known at "toe thrusts" that are formed as sediment flows downslope (Shankar and Riedel, 2010). These ridges (e.g. Ridges A, B, C in Figure 10A) result in secondary slope basins that trap sediment, resulting in large spatial variations in the recent sedimentation rate.

Krishna-Godavari basin - Apparent Heat Flow

A swath bathymetric map of the K-G basin was available to us, allowing higher resolution bathymetric mapping than was possible in the other two study areas, where only seismic bathymetry was available (Figure 10A). The K-G basin seismic volume extends from water depths of 600 to 1800 m, with BSRs present in water depths of 800 to 1300 m. Seafloor temperatures in the K-G basin range from 3 to 8°C in the region of the seismic survey (Figure 7A). For a thermal conductivity of 0.95 W/m^2, apparent heat flow in the K-G basin ranges from 0.024 W/m^2 to 0.06 W/m^2 (Figure 10B). The thermal conductivity data from the NGHP-01 core samples do not allow us to resolve variable thermal conductivity. The variations in apparent heat flow, however, are larger than the variations due to uncertainties in thermal conductivity and other parameters.

To test whether the apparent increase in temperature gradient with increasing water depth observed in the borehole temperature data (Figure 1C) is a regional feature or an artifact of the limited spatial coverage provided by the borehole data, we divided the region into several slices and plotted the apparent heat flow as a function of water depth color-coded by region (Figure 11).

The northeast part of the survey shows an irregular patter of apparent heat flow, with local highs and lows. A major topographic ridge through this region (labeled Ridge A in Figure 10A) is associated with a heat flow low (Figure 12A-C). Two-dimensional

modeling using the method of Lachenbruch (1968) indicates that the trough in the apparent heat flow can be attributed to refraction of conductive heat flow by Ridge A (Figure 12D). Local highs have been associated with faults by Yu et al. (unpublished manuscript) and interpreted as conduits for advective flow, which brings warmer fluids from below, locally shoaling the BSR. See Dewangan et al. (2011) and Shankar and Riedel (2010) for additional examples of seismic data in this region. In summary, local variations in heat flow in the NE part of the K-G basin study area are dominated by local topography and faulting and there is no significant regional correlation between topography and heat flow here (Figure 11B). Average apparent heat flow in this region is ~0.04 W/m^2.

The southwest portion of the study area (regions color-coded by red and blue in Figure 11A) is dominated by relatively low heat flow in the north, rimmed to the southeast by higher heat flow. Seismic reflection profiles show that in this region, a sediment basin is accumulating bounded by Ridge B to the south (Figure 10A). Sediments are ponded behind this ridge (Figure 10C), leading to increasing sedimentation rate from the ridge to the basin. In the section on modeling, we examine quantitatively whether a 3-fold increase in sedimentation rate in this basin can explain the apparent down-slope increase in heat flow across this part of the K-G basin from ~0.03 W/m^2 in 975 m to 0.045 W/m^2 in 1100 m.

Sites 7 and 16 (Figure 1C), located ~70 km NE of the primary seismic survey and in water depth of ~1300 m (Table 1), show somewhat higher heat flow. Although the borehole data indicate that this is unlikely to be due to different sediment properties, the reason for this observation was not explored further because of the lack of seismic data to link the stratigraphic and structural setting of these two sites to the rest of the K-G basin sites.

Mahanadi basin - Apparent Heat Flow

Mahanadi basin is located to the northwest of K-G basin, along the eastern Indian passive margin (Figure 1A) and likely has a similar geologic history. Seismic surveys were performed at two sites within the Mahanadi basin; however, only one of those sites exhibited a clear BSR. The seismic survey where the BSR was present comprised two perpendicular swaths, with each swath consisting of three closely-spaced lines. Lacking swath bathymetry, bathymetry was constructed from two-way travel times (Figure 13A). Seafloor temperatures over the study are from World Ocean Atlas 2005 (Figure 8B). Seafloor depths where BSRs were present range from 1500 to 1750 m, with seafloor temperatures ranging from 3 to 5°C. Apparent heat flow was calculated for the Mahanadi Basin using a sediment velocity of 1550 m/s (Figure 13B). A thermal conductivity value of 0.95 was used to calculate heat flow. The Mahanadi basin exhibits a positive correlation between water depth and heat flow (Figure 13C); however, the amplitude of the variation is barely larger than uncertainty in the heat flow as estimated from the

uncertainty of the parameters used to calculate it, and we cannot rule out a systematic down-slope change in these parameters in such a way that heat flow would appear to increase down-slope even if actual heat flow were constant.

Andaman Basin - Geologic Setting

The Andaman basin is a forearc basin located just west of the Andaman Islands in the western Bay of Bengal (Figure 1A). The geologic and tectonic setting of this region has recently been reviewed by Cochran (2010). Subduction along this segment of the Sumatra subduction zone was initiated ~65 Ma and is currently highly oblique. As is common for highly oblique subduction zones, there are few active volcanoes along this segment of the arc, unlike further to the southeast, where there is a vigorous volcanic arc on the island of Sumatra. Instead, the backarc is characterized by strike-slip faulting and possibly backarc extension (Figure 2A).

Site 17 was located on the eastern flank of a forearc high that emerges above sea level in the Andaman Islands. Seismic reflection profiles show a thick package of sediments with complex folding and faulting in this region (Figure 2B). Site 17 is on a local ridge that has been interpreted to be a fault marking the boundary between the forearc high and the forearc basin to the east, shown in Figure 2A as the Diligent Ridge. The eastern edge of this basin corresponds to the West Andaman Fault, a very seismically active strike-slip fault that joins the active volcanic arc on Sumatra. Cochran (2010) speculates that the region between the Eastern Margin Fault and the West Andaman Fault is analogous to the Aleutian forearc basin, which is thought to have formed because of subduction erosion, which thinned the basement crust from below.

Sediments retrieved at Site 17 indicate that terrigenous sediment input is low, but that volcanic activity has produced numerous ash layers. While hydrates in small concentrations were present throughout the pore space, high gas hydrate concentrations were restricted to the ash layers. Ash layers showed higher porosity as a result of increased grain size, allowing for greater fluid flow and more space in which hydrate can grow (Collett et al. 2008). Carbon isotopes indicate the presence of both thermogenic and biogenic methane sources.

Andaman basin - Apparent Heat flow

Overall, the Andaman basin exhibits a surprisingly deep BSR. Borehole temperature measurements, which indicated a very low thermal gradient of 19°C/km, confirmed that the observed BSR at 608 mbsf is the base of the gas hydrate stability zone and not the Opal-CT transition, as had been hypothesized prior to drilling and measurement of in situ temperature (Collett et al 2008). Shipboard thermal conductivity measurements (Figure 7) indicate an average thermal conductivity of ~0.90 $Wm^{-1}K^{-1}$ above the BSR, resulting in a heat flow of 0.017 W/m^2. Low heat flow is a common characteristic of forearc

basins, which often have heat flow that is, on average ~60% of the heat flow expected for lithosphere that has the age that the subducting plate has at the trench (Stein, 2003). This depression of forearc heat flow is generally understood to be a result of thickening of the overriding plate as the subducted plate descends into the mantle. Given the age of the subducting plate in this region (~70 Ma), the expected heat flow is 60% of 0.60 W/m^2. The observed heat flow at Site 17 is significantly less and near the low end of global observations (Stein, 2003). In the modeling section, we examine whether the apparent heat flow here may be further depressed by very high recent sedimentation rates.

Andaman basin bathymetry was constructed from seafloor depths derived from seismic data, as swath bathymetry was unavailable (Figure 14A). NGHP site 17 is located on a ridge in the western portion of the study area. Seafloor temperatures in the Andaman basin range from 2 to 8°C (Figure 8C). Figure 14B shows BSR-derived apparent heat flow for the Andaman basin. High apparent heat flow regions tend to be found in deeper areas, while lower heat flow is found along ridges and in the shallower western portion of the study region. As in the NE part of the K-G basin study area, the heat flow is correlated with local ridge and trough topography, suggesting that variations are dominated by refraction of heat by topography. Relatively high heat flow is also observed in the southeast part of the survey and will be discussed later. An apparent circular local high is likely an artifact due to misidentification of the BSR in a region of intermittent BSR occurrence.

When plotted as a function of water depth, heat flow in the Andaman basin increases as a function of depth (Figure 15), and the heat flow at NGHP site 17 is within one standard deviation of the average binned apparent heat flow value. Figure 15 also includes a histogram of the number of data points in each depth bin. The scatter in the points decreases as the number of data points decreases, indicating that the sample size is not large enough to adequately define the uncertainty due to scatter in the data points. Note that this estimate of uncertainty does not include the estimated 10% uncertainty in parameters that are assumed to be constant in the calculation.

Margin Heat Flow Compilation

In order to place the Indian margin and Andaman basin in a global context, we compiled heat flow as a function of water depth for five margins, both passive and active (Figure 16). Heat flow from other regions was collected through two means, from traditional bowstring seafloor heat flow measurements or from BSR derived heat flow. The K-G basin, Mahanadi basin, Andaman basin, Nankai trough, Hikurangi basin, Blake ridge, and Makran accretionary prism were included for comparison based on availability and documentation in literature (Kaul et al. 2000; Ruppel et al. 1995; Townend 1997; Yamano et al. 1982). Additional margins were pulled from the Global Heat Flow Database (GHFD), compiled most recently by Hasterok (2010). The GHFD represents traditional probe data worldwide, and was filtered based on margin setting and seafloor

depth at probe site. Only measurements made on the continental slope from 200 to 3200 meters below sea level (mbsl) were used, and the geographic selections avoided hotspots and spreading centers. The number of measurements available at each margins varied considerably, from the tens to hundreds of measurements. Regions that had few measurements, such as the Bay of Bengal, were not included in the compilation.

The data and resulting best-fit lines all show increasing heat flow with increasing depth although the slopes, as well as the average heat flow, vary considerably from margin to margin (Figure 16C). For the West African and West Indian margins the difference between shallow and deep water is within the uncertainty of the observations. For the K-G basin, we showed that the heat flow versus depth relationship depends strongly on the subset of data used, and that patterns within subsets could be explained in large part by local features. This is also suggested by the different slopes shown for eastern North America as a whole and for the Blake ridge, which is a part of the margin of eastern North America. It is likely that the global observation of an increase in heat flow with increasing water depth on passive margins is dominated by local structural and stratigraphic history.

The relationship is more robust for active margins, which generally show similar slope (Figure 16D). Here the increase in apparent heat flow with increasing water depth likely reflects the decrease in heat flow that results as a subducting plate is progressively covered by a thickening accretionary prism; the intercept likely depends on the age of the subducting plate, with a younger subducting plate leading to higher average heat flow. However, the slope and average also depend strongly on the subset of data used, as shown by the different results for the ensemble of Cascadia heat flow values from probe data and the Cascadia BSR transect, which was taken from the central part of the subduction zone where the subducting plate is oldest, explaining why the average heat flow is lower. The Cascadia-wide compilation from GHFD may also be biased to higher values by incorporation of observations from the abyssal plain seaward of the trench because of the relatively shallow depth of the abyssal plain here, which is <3200 m where affected by deep sea fans. The intercept for the Andaman basin, however, is the lowest of all the active margins, highlighting the anomalously nature of the low heat flow here.

Modeling the effects of variable sedimentation rate and fluid flow

To obtain a quantitative estimate of the effects of sedimentation on apparent heat flow, we constructed a series of one-dimensional conductive models with sedimentation rates constrained by the drilling data. Our objective with this modeling was to determine whether the lateral variations we noted in the previous section are within the range that can be attributed to the effects of sedimentation and topography on conductive heat flow or whether large-scale convective heat transport is required. We did not address local convective heat transport along faults because that has been discussed in recent papers by

others (Shankar and Riedel, 2010; Dewangan et al., 2011; Yu et al., unpublished manuscript).

Both sedimentation and erosion affect conductive heat flow. High sedimentation rates will decrease near-surface heat flow estimates while erosion exposes warmer sediments, resulting in higher near-surface heat flow estimates. Sedimentation rates in the K-G and Mahanadi basins are unconstrained by borehole biostratigraphic datums. (Collett et al, 2008). Sedimentation rates of 20 to 25 cm/ky (Rao et al., 1994) are applicable only from Paleocene to present, prior to which sedimentation rates were lower, although how much lower is unknown (Subrahmanyan and Chand, 2006). Biostratigraphic datums at Site 17 in the Andaman basin show an average sedimentation rate of 7 cm/ky (Figure 17). Topography also affects heat flow, with heat being focused away from topographic highs and into troughs (Lachenbruch, 1968; Blackwell, 1980).

Porosity and compaction

Compaction must be taken into account when calculating sedimentation rate from biostratigraphic datums. Compaction results in a decrease in porosity with increasing depth. In the absence of major lithologic changes, the porosity versus depth profile in sediments is expected to follow an exponential curve (Hyndman and Wang, 1993, Bahr et al, 2001, Torres et al, 2004).

Porosity at the surface ($phi_{surface}$) was calculated from drilling data. Assuming a lithologically-defined lower porosity limit of 20% the following equation was used to determine compaction (from Torres et al, 2004):

$$phi_z = phi_{inf} + (phi_{surface} - phi_{inf}) \times e^{(-z \times phi_{depthscale})} \quad \text{(Eq. 3)}$$

where z is depth, phi_{inf} is the porosity at infinity, $phi_{surface}$ is the surface porosity for which a value of 0.68 was used in all calculations, and $phi_{depthscale}$ is the compaction coefficient, and defines the rate at which compaction takes place (Figure 17A,C).

Site 17 exhibited an unusual porosity depth profile, with the upper 200 m following a steep exponential curve, under which there is an abrupt increase in porosity that remains consistently high for the remaining 500 m of the borehole (Figure 17A). Initially we thought this might be the result of dissociating disseminated hydrate creating gas pockets in core samples as they equilibrated to atmospheric conditions. However this feature is also present in the in-situ logging profiles (Figure 17B). A porosity increase at depth is typical for over-pressured sediments. Over-pressurization can be caused by either high sedimentation rates or by a formation capped by an impermeable layer. Both of these scenarios would likely be associated with a lithologic change; however, even though recovery at 200 mbsf was high, likely capturing any potential variation, no apparent lithologic change was observed by the shipboard sedimentologists (Collett, 2008).

In the K-G basin, borehole porosity profiles are consistent with a shale-dominated environment (Bahr et al, 2001). Porosity and compaction coefficients used for K-G basin modeling were derived from the Site 3 porosity profile (Collett et al., 2008), which was typical of K-G basin sites.

Andaman basin models

Multiple scenarios were considered that could potentially explain the anomalously low heat flow exhibited at site 17 in the Andaman Basin. The 1D model of Hutchison (1985) as coded by Kelin Wang (Pacific Geoscience Center, Canada), calculates heat flow and depth as a function of plate age for a specified sedimentation history. Parameters to specify include thermal properties of sediment, crust, and mantle, a multistage sedimentation history, compaction parameters, densities of materials, and heat generation. Parameter values used in all models can be found in Table 1. Basement age, sedimentation rate, and total sediment thickness were varied in an attempt to reconstruct the anomalously low heat flow exhibited at site 17.

The age of the subducted plate beneath the forearc is estimated to be ~75 to 80 Ma based on projecting the Caltech Tectonics Group map of seafloor age (2009). Forearc basement age in the Andaman Basin, however, is unknown, and it is unclear whether the underlying basement is of continental or oceanic origin (Cochran, 2010). Another poorly constrained variable used in model construction is basement depth. The Andaman Basin is a relatively poorly understood region, where basement depth is only defined by a 3D gravity inversion of the Andaman region performed by the Directorate General of Hydrocarbons of India. Cochran (2010) shows a seismic profile across site 17, which extends to 8 seconds of two-way travel time and does not show a basement reflection, putting a constraint on minimum basement depth of 10 km assuming an average sediment velocity of 2.5 km/s. However, it is unclear whether the basement is unresolved because the maximum depth does not extend far enough to see the basement reflector, or whether the seismic source used was not powerful enough to resolve basement.

The geothermal gradient in the upper 700 m at site 17 is perhaps the best-constrained variable, independently verified by BSR derived thermal gradient and by in-situ borehole temperature measurements taken during drilling operations. The thermal gradient at site 17 is 19°C/km. Sedimentation rate for the past 10 My is also well constrained. Post cruise biostratigraphy resulted in a revision of the shipboard datums (Collett et al., 2008), increasing the depth where sedimentation rates are constrained from 108 m in the initial reports, to 700 m, the entire length of the borehole (Flores et al., 2008; Cawthern et al., 2010). This increased the initial estimate of 5.6 cm/ky over the upper 108 m to 7 cm/ky over the entire borehole (Figure 17). Figure 19 shows the effect of changing the recent sedimentation rate from the rate given in the Initial Report (blue line) to the updated rate (red line). The blue line fit the data assuming 1.2 My with a very fast sedimentation rate

of 2000 cm/ky prior sandwiched between a 70 My at 10 cm/yr prior to the pulse of high sedimentation rate and 2 My at 10 cm/yr afterwards. Adding an additional 7 My of slower sedimentation to the recent sedimentation history results in additional rebound of the predicted thermal gradient. Because we did not learn of the new biostratigraphic constraints until December 2010 (the initial project end date), we did not have time to adjust model parameters to fit the data. However, given the limited detailed constraints on tectonic history and non-uniqueness of the solution, it is likely that a reasonable model could be obtained by adjusting the duration of the period of very fast sedimentation, which is a 1D model proxy for tectonic thickening.

The temporal evolution of surface heat flow predicted by this model is shown in Figure 20 compared to a model of an unsedimented, cooling oceanic lithosphere as well as to the GDH1 model of heat flow as a function of plate age (Stein and Stein, 1992). Our modeled scenario follows the trend of both the unsedimented model and the GDH1 model until the sedimentation rate increases from 10 cm/ky to 2000 cm/ky at ~70 My, at which time there is a sharp drop in apparent heat flow. This drop is followed by a rise resulting from lowering the sedimentation rate as determined from the updated borehole age model. A line showing 50% of GDH1 is also shown because Stein (2003) has shown that heat flow in forearc basins is generally 50-60% lower than what would be expected for lithosphere having the age of the lithosphere at the trench (Figure 20B). The data from the Andaman basin is clearly lower, perhaps because of an unusually fast forearc thickening rate combined with fast sedimentation.

Krishna-Godavari basin models

In the K-G basin, we addressed 2 questions through modeling. First we used the 1D model for the effect of sedimentation to evaluate whether sedimentation could explain the apparent increase in heat flow in the SW part of the study area, where a recent slope basin is forming behind a thrust ridge and sedimentation rate increases as water depth decreases. Second we used the 2D analytic model of Lachenbruch (1968) to see if the amplitude of the anomaly associated with Ridge A (Figure 10A) in the NE part of the study is consistent with topographic refraction. Recall that data from the NE part of the study area do not show a significant correlation between apparent heat flow and water depth. Instead, the average heat flow of ~0.04 W/m^2 is similar to that expected for lithosphere that rifted in the Mesozoic (Figure 20A), and local variations likely result from fluid flow along local faults or from refraction of conductive heat flow due to local topography.

No biostratigraphic constraints were available for the SW K-G basin due to shallow boreholes and the absence of dateable biostratigraphic markers (Collett et al., 2008). Sedimentation rates of 20-25 cm/ky have previously been found for the region, (Rao et al., 1994), and a sedimentation rate of 22 cm/ky was used in modeling efforts.

Plate age and basement depth were obtained from the Hasterok et al. (2010) Worldmap program. Sediment thickness found using this program is between 8000 and 9000 m, which agrees with that reported by Collett et al. (2008). Plate age from Worldmap is 120 My, which agrees with Subrahmanyam et al. (1999) dating of 118 to 132 Ma from magnetic anomalies.

The geothermal gradient in the K-G basin is well constrained from BSR derived heat flow and borehole temperature measurements. Here we used the average regional heat flow value for the K-G basin of 0.04 W/m^2 in model comparisons. The regional conductive heat flow model produced for the K-G basin using the above variables results in a surface heat flow of 0.036 W/m^2 and a sediment thickness of 8600 m (Figure 21A and 21B). Lowering the sedimentation rates to 10 cm/ky prior to 65 Ma, as suggested by Subrahmanyam and Chand (2006), decreases the heat flow to 0.035 W/m^2, given a basin thickness of 7800 m. This shows that regional average sedimentation rates through the history of the basin have not been large enough to have a major effect on heat flow. From this we conclude that large-scale regional fluid flow rates are too low to have a significant effect on the shallow thermal gradient. Prior studies (e.g. Tréhu et al., 2003; Torres et al., 2004) indicate that this rate less than ~0.1 cm/yr.

The low heat flow region in the SW part of the study is correlated with a basin bounded to the south by a ridge formed by a toe thrust. Models were constructed to determine if higher sedimentation rates behind the ridge could be responsible for correlation between heat flow and water depth in this region. Based on the geometry of seismic horizons (Figure 21), sedimentation rates in the northwest basin are three times higher than sedimentation rates on the ridge, so a sedimentation rate of 75 cm/ky was used to model heat flow in the basin. The basin thickness is at least 800 m (the base of the basin is below the base of the seismic data), corresponding to a basin age of 1.1 Ma. Assuming a sedimentation rate of 75 cm/ky for the last 1.1 My reduced the surface heat flow to 0.0345 W/m^2. Increasing the estimated basin age to 11 My reduced the surface heat flow to 0.032 W/m^2. Increasing sedimentation rate to 500 cm/ky results in a heat flow of 0.028 mW/m^2. We consider this rate to be unlikely. This exercise shows that sedimentation in the basin can depress heat flow can account for ~1/2 of the apparent depression of heat flow as water depth decreases over the basin. The remaining difference between the model and the observations could be due to differences in thermal conductivity if basin sediments are more clay-rich than those of the ridge. Alternatively, it could be due to lateral heat advection.

NGHP-01 Sites 10, 11, and 12 were drilled on the ridge structure (Figure 10), and showed the most concentrated methane hydrate deposits. The apparent heat flow at this site is ~0.050 W/m^2, which is slightly higher than the background flow rate of 0.040 W/m^2. Previous studies have shown that fault networks could be responsible for this concentration through fluid migration along the faults (Dewangan et al., 2011). These

faults intersect the subhorizontal horizons underlying the basin providing a possible path for lateral advection of heat transport from beneath the basin to the ridge (Figure 22).

Using a 1D vertical fluid advection model (Turcotte and Schubert, 2002), we examined the impact of near-vertical fluid flow on apparent heat flow to determine the rates needed to explain the high apparent heat flow here. For the 1D flow model:

$$T = Tr - (Tr - To)\exp((\rho_f c_f v_f/k)y) \quad \text{(eq. 4)}$$

where T is temperature, Tr is the temperature in a fluid reservoir at great depth, To is the surface temperature, ρ_f is fluid density, c_f is the specific heat of the fluid, k is the thermal conductivity of the sediment and v is the fluid velocity.

Assuming k = 0.95 W/(mK), $c_f = 4.185 \times 10^3$ J/(kgK), $\rho_f = 1028$ kg/m^3, the effect of fluid velocities ranging from 0.01 to 10 cm/yr (black dashed lines) is shown in Figure 22A compared to the borehole data at Site 10 and to the regional background thermal gradient of 0.042 K/m (red line) and the best-fit thermal gradient at Site 10 of 0.052 K/m (blue line). The methane hydrate stability boundary (Sloan and Koh, 2007) and depth to the BSR are also shown and are consistent with the observed thermal gradient. The dashed red line shows the effect of fluid flow at 0.1 cm/yr added to the background gradient and fits the data well. Note that for velocities <0.1 cm/yr, the effect of flow on the thermal gradient is very small; for flow rates of 0.1-1 cm/yr, the impact on the thermal gradient in the upper few 100 meters is nearly linear and cannot be distinguished from advection heat transport based on the characteristic curvature of the temperature profile; for flow rates > 1 cm/yr, we would not expect to see a BSR in the region of flow because of elevated temperature. This latter situation is seen in place on the Cascadia margin where the BSR comes to the surface beneath vents (e.g. Wood et al., 2002).

Figure 22B shows the effect of fluid velocity in the range 0.1-0.6 cm/yr along with the effect of uncertainty in the thermal parameters (k = 0.9-1.0 W/(mK); cf = 2.5 - 4.185 x 10^3 J/(kgK), where the lower value is the specific heat of wet mud and the higher value is the specific heat of fresh water). The thermal perturbation due to flow in this simple model is very sensitive to fluid velocity in this range and insensitive to uncertainties in the thermal properties of the subsurface. We conclude that fluid velocities of ~0.1 cm/yr can explain the locally elevated thermal gradient beneath Ridge B, which is a buried ridge with only a very subtle topographic manifestation (Figure 10A). This contrasts with Ridge A, which corresponds to a heat flow low that can be explained by topographic refraction (Figure 12C). Other local apparent heat flow highs in Figure 10B are likely caused by similar small anomalies in fluid flow along faults. Note that nowhere in our data do we see the dramatic shallowing of the BSR predicted by flow velocities > 1 cm/yr. Given the small amplitude of the anomalies, the low flow rates implied, and uncertainties in physical properties of the sediments, we considered that a more sophisticated 3D fluid/heat transport model was not justified by these data.

Conclusions

Downhole temperatures measured during NGHP-01 predicted the depth to the base of the gas hydrate stability zone to within a few meters of the depth predicted from seismic observations of the BSR at all sites for which both a BSR and in-situ temperature measurements were available. We therefore used the seismic surveys and measurements of seismic velocity, density and thermal conductivity, along with information on bottom water temperature from the World Ocean Atlas, to generate apparent heat flow maps of the K-G, Mahanadi and Andaman basins. The K-G and Mahanadi basins are on the ~125 million year old rifted margin of India and the Andaman basin is in the forearc of the Sumatra subduction zone. We estimate that uncertainty in the heat flow is as much as 10% due to uncertainty in the physical properties of the sediment and pore water and gas chemistry. Half of this uncertainty results from uncertainty in thermal conductivity, which likely changes slowly due to changing lithologic regimes, so local trends in heat flow are probably more robust than would be indicated by this estimate.

When all data are taken together, a correlation between increasing heat flow and increasing water depth is observed that is similar to what is observed from active and passive continental margins worldwide and is opposite the observed correlation between increasing water depth and decreasing heat flow observed in ocean basins due to lithospheric cooling and contraction as a function of age. We examined this relationship in more detail to determine whether we could derive any regional insights into the fluid flow regimes that control the distribution of gas hydrates in these environments.

The results indicate that the K-G basin is characterized by two distinct heat flow regimes. In the northeastern part of the study area, heat flow is quite variable and shows a distinct trough in the heat flow that is coincident with a topographic ridge. Simple 2D analytic modeling indicates that the heat flow variability here is likely due to refraction of conductive heat flow by the topography. Local heat flow highs in this region are likely associated with fluid flow along faults. While these two processes lead to scatter in the data from this region, there is no significant heat flow versus water depth relationship in this region. In the southwest region, low heat flow is associated with a sedimentary basin formed as sediments are trapped behind a ridge that is the result of slumping and development of a toe thrust at the seaward edge of a massive sediment pile formed from the deltas of the Krishna and Godavari rivers. This results in a correlation between increasing heat flow and increasing water depth because water depth decreases as the basin thickens. Modeling of sedimentation indicates that ~50% of the heat flow versus water depth relationship here is due to variable sedimentation rate. If the basin sediments have lower thermal conductivity than the sediments forming the ridge, then even more of the anomaly can be attributed to conductive processes, leaving only a small heat flow perturbation that can be attributed to advective heat transport. We speculate that fluids

may migrate along stratigraphic horizons towards the ridge, where they then find their way to the surface along steeply-dipping fractures that are imaged in the seismic data and are where hydrate deposits sampled during NGHP-01 are concentrated. A small increase in heat flow from the regional background value of 0.04 W/m^2 to 0.05 W/m^2 beneath the buried ridge that hosted the richest hydrate deposits sampled during NGHOP-01 is consistent with a fluid flow rate of ~0.1 cm/yr.

At ~0.017 W/m^2, the one borehole heat flow measurement in the Andaman basin (Site 17) is on the low end of global observations from continental margins. This very low heat flow results in an unusually thick gas hydrate stability zone. The heat flow map derived from BSR data constrained by this one borehole indicates that this very low heat flow is regional, although there are variations due to local topography and apparent heat flow increases with water depth. In general, heat flow in forearc basins is depressed by up to 50% compared to the heat flow predicted for the plate age at the trench. In the Andaman basin, the heat flow is depressed ~65% compared to heat flow for oceanic lithosphere of the expected age. This very low heat flow results in a very thick hydrate stability zone throughout this region.

Acknowledgements

We thank the scientists, technicians and crew of the D/V JOIDES Resolution for the success of NGHP Expedition 01. We thank Seismic Microtechnology for their donation of Kingdom Suite seismic interpretation software, with which seismic evaluations and gridding were performed. This research is supported by Department of Energy – National Energy Technology Laboratory award no. DE-NT0005669.

References

Bahr DB, Hutton E, Syvitski J, Pratson L (2001) Exponential approximations to compacted sediment porosity profiles, Computers and Geosciences, 27, 691-700

Bangs, NLB, Sawyer, DS, Golovchenko (1993) Free gas at the base of the gas hydrate zone in the vicinity of the Chile triple junction, Geology, 21, 905-908.

Blackwell, DD, Steele, JL, Brott CA (1980) The terrain effect on terrestrial heat flow, J. Geophys. Res., 89, 4757– 4772.

Cawthern T, Johnson JE, Bryce J, Blichert-Toft J (2010) A ~10 Ma petrochemical record from the Andaman accretionary wedge: implications for arc evolution. Abstract V14A-04 presented at 2010 Fall Meeting, AGU, San Francisco, Calif., 13-17 Dec.

Cochran JR (2010) Morphology and tectonics of the Andaman Forearc, northeastern Indian Ocean. Geophysical Journal International, 182: 631–651.

Collett TS, Riedel M, Cochran J, Boswell R, Presley J, Kumar P, Sathe A, Lall M, Sibal V, and the NGHP Expedition 01 Scientists (2008) National Gas Hydrate Program Expedition 01 initial report, Dir. Gen. of Hydrocarbons, Minist. of Pet. and Nat. Gas, New Delhi.

Davis EE, Villinger H, MacDonald RD, Meldrum RD, Grigel J (1997) A robust rapid-response probe for measuring bottom-water temperatures in deep-ocean boreholes. Mar. Geophys. Res. 19:267-281,

Dewangan P, Sriram G, Ramprasad T, Ramana MV, Jaiswal P (2011) Fault system and thermal regime in the vicinity of site NGHP-01-10, Krishna-Godavari basin, Bay of Bengal, Marine and Petroleum Geology, In Press, Corrected Proof, ISSN 0264-8172, DOI: 10.1016/j.marpetgeo.2011.03.009.

Dugan B, Flemings PB (2000) Overpressure and fluid flow in the New Jersey continental slope: implications for slope failure and cold seeps. Science 289:288-291.

Flores J-A, Mejía-Molina AE, Álvarez C, Sierro FJ, Giosan L, Johnson JE (2008) Calcareous nannofossil biostratigraphy from sediment cores recovered in the Arabian Sea, Bay of Bengal, and Andaman Sea during NGHP Expedition 01. International Conference on Gas Hydrates, Noida India, Feb. 6-8, 2008.

Ganguly N, Spence GD, Chapman NR, Hyndman RD (2000) Heat flow variations from bottom simulating reflectors on the Cascadia Margin. Marine Geology 164:53-68.

Grevemeyer I, Villinger H (2000) Gas hydrate stability and the assessment of heat flow through continental margins. Geophys. J. Int. 145:647-660.

Gupta, SK (2006) Basin architecture and petroleum system of the Krishna Godavari Basin, east coast of India, The Leading Edge, 25, 830.

Hasterok, D (2010) Thermal state of continental and oceanic lithosphere, PhD thesis, University of Utah, U.S.

He L, Wang J, Xu X, Liang J, Wang H, Zhang G (2009) Disparity between measured and BSR heat flow in the Xisha Trough of the South China Sea and its implications for methane hydrate. Journal of Asian Earth Sciences 34:771-780.

Heesemann M, Villinger H, Fisher AT, Tréhu AM, White S (2006) Data report: testing and deployment of the new APCT-3 tool to determine in situ temperatures while piston coring. Proceedings of the Integrated Ocean Drilling Program, Vol. 311.

Hutchison I (1985) The effects of sedimentation and compaction on oceanic heat flow. Geophysical Journal of the Royal Astronomical Society, 82(3), 439-459.

Hyndman RD, Wang K, Yuan T, Spence GD (1993) Tectonic sediment thickening, fluid expulsion, and the thermal regime of subduction zone Accretionary prisms: The Cascadia Margin off Vancouver Island. J. Geophys. Res. 98:21865:21876.

Hyndman, RD, Wang, K, (1993) Thermal constraints on the zone of major thrust earthquake failure: The Cascadia subduction zone: J. Geophys. Res., 98, 2039–2060.

Kaul N, Rosenberger A, Villinger H (2000) Comparison of measured and BSR-derived heat flow values. Makran accretionary prism, Pakistan. Marine Geology 164:37-51.

Korenaga, J, Holbrook, WS, Singh, SC, Minshull, TA (1997) Natural gas hydrates on the SE US margin: constraints from full waveform inversion of wide-angle seismic data, J. Geophys. Res., 102, 15,345-15,365.

Lachenbruch, AH (1968) Rapid estimation of the topographic disturbance to superficial thermal gradients, Reviews of Geophysics, 6, 365-400.

Locarrini RA, Mishonov AV, Antonov JI, Boyer TP, Garcia HE (2006) World Ocean Atlas 2005, Volume 1: Temperature. S. Levitus, Ed. NOAA Atlas NESDIS 61, U.S. Government Printing Office, Washington, D.C.

Maekawa T, Itoh S, Sakata S, Igari S, Imai N (1995) Pressure and temperature conditions for methane hydrate dissociation in sodium chloride solutions. Geochemical Journal 29:325-329.

Martin V, Henry P, Nouze H, Noble M, Ashi J, Pascal G (2004) Erosion and sedimentation as processes controlling the BSR-derived heat flow on the Eastern Nankai margin. EPSL 222:131-144.

Murthy, KSR, Subrahmanyam, AS, Lakminarayana, S., Chandrasekhar, DV, Rao, TCS (1995) Some geodynamic aspects of the Krishna-Godavari basin, east coast of India, Continental Shelf Research, 15, 779-788.

Rao DP, Bhattacharya GC, Ramana MV, Subrahmanyam V, Ramprasad T, Krishna KS, Chaubey AK, Murty GPS, Srinivas K, Desa M (1994) Analysis of multi-channel seismic reflection and magnetic data along 13N latitude across the Bay of Bengal. Mar. Geophys. Res. 16:225–236.

Rao GN (2001) Sedimentation, stratigraphy, and petroleum potential of the Krishna-Godavari basin, East Coast of India. AAPG Bulletin, 85:1623-1643.

Riedel M, Collett TS, Kumar P, Sathe AV, Cook A (2010) Seismic imaging of a fractured gas hydrate system in the Krishna-Godavari Basin offshore India, Marine and Petroleum Geology, 27, 1476-1493.

Ruppel C, Von Herzen RP, Bonneville A (1995) Heat flux through an old (~175 Ma) passive margin: Offshore southeastern United States. Journal of Geophysical Research, 100, 20037-20057.

Shankar, U, Riedel, M (2010) Seismic and heat flow constraints from the gas hydrate system in the Krishna-Godavari basin, India, Marine Geology, 276, 1-13.

Shipley, TH, et al. (1979) Seismic reflection evidence for the widespread occurrence of possible gas-hydrate horizons on continental slopes and rises, Am. Assoc. Petrol. Geol. Bull., 63, 2204-2213.

Singh SC, et al. (2008) Seismic evidence for broken oceanic crust in the 2004 Sumatra earthquake epicentral region. Nature Geoscience, 1(11), 777-781.

Sloan ED, Koh C (2007) Clathrate hydrates of natural gases, Third Edition, CRC Press.

Stein, CA (2003) Heat flow and flexure at subduction zones, Geophys. Res. Lett., 30, doi 10.1029/2003GL018478.

Stein, C, Stein, S (1992) A model for the global variation in oceanic depth and heat flow with lithospheric age, Nature, 359, 123-128

Subrahmanyam C, Chand S (2006) Evolution of the passive continental margins of India--a geophysical appraisal, Gondwana Research, 10(1-2), 167-178, ISSN 1342-937X, DOI: 10.1016/j.gr.2005.11.024.

Subrahmanyam C, Thakur NK, Rao TG, Khanna R, Ramana MV, Subrahmanyam V (1999) Tectonics of the Bay of Bengal: new insights from satellite-gravity and ship-borne geophysical data, Earth and Planetary Science Letters, 171(2):237-251, ISSN 0012-821X, DOI: 10.1016/S0012-821X(99)00148-X.

Torres ME, Wallman K, Tréhu AM, Bohrmann G, Borowski WS, Tomaru H (2004), Gas hydrate growth, methane transport, and chloride enrichment at the southern summit of Hydrate Ridge, Cascadia margin off Oregon, Earth and Planetary Science Letters Vol. 226: 225-241.

Townend J (1997) Estimate of conductive heat flow through bottom-simulating reflectors on the Hikurangi and southwest Fjordland continental margins, New Zealand. Marine Geology 141:209-220.

Tréhu AM (2006) Subsurface temperatures beneath southern Hydrate Ridge. In Tréhu, AM, Bohrmann G, Torres ME, Colwell FS (Eds.) Proc ODP, Sci. Res., 204:1-26.

Tréhu AM (2007) Preliminary results from in situ temperature measurements made during NGHP-01 (extended abstract for the NGHP-01 post-cruise meeting, Noida, India.

Tréhu AM, Long PE, Torres ME et al. (2004) Three-dimensional distribution of gas hydrate beneath southern Hydrate Ridge: constraints from ODP Leg 204, Earth and Planetary Sciences, 222:845-862.

Tréhu AM, Lin G, Maxwell E, Goldfinger C (1995) A seismic reflection profile across the Cascadia subduction zone offshore central Oregon: New constraints on methane distribution and crustal structure. J. Geophys. Res., 100:15101-15116.

Turcotte DL, Schubert G (2002) Geodynamics, 2nd ed. Cambridge University Press. Cambridge, New York, Melbourne.

Villinger, H, Tréhu, AM, Grevemeyer, I (2010) Seafloor marine heat flux measurements and estimation of heat flux from seismic observations of bottom simulating reflectors, in press, SEG special issue on geophysics and gas hydrates.

Wong GSK, Zhu S (1995) Speed of sound in seawater as a function of salinity, temperature and pressure. J. Acoust. Soc. Am. 97:1732-1736

Wood, W. T., J. Gettrust, N. R. Chapman, G. D. Spence, and R. D. Hyndman, Decreased stability of methane hydrates in marine sediments due to phase boundary roughness, Vol 420, Nature, Dec 12, 2002.

Yamano M, Uyeda S, Aoki Y, Shipley TH (1982) Estimates of heat flow derived from gas hydrates. Geology 10:339-343.

Yu P, Riedel M, Shankar U, Collett TS, Sathe AV, Structural interpretation of large-scale faulting in the Krishna-Godavari Basin offshore India to define gas migration pathways for hydrate formation. (in review).

Xu, W, Ruppel, C (1999) Predicting the occurrence, distribution, and evolution of methane gas hydrate in porous marine sediments, J. Geophys. Res., 104, 5081 – 5096.

Zwart, G, Moore, JC, Cochrane, GR (1996)Variations in temperature gradients identify

active faults in the Oregon accretionary prism, Earth Planet. Sci. Lett., 139, 485 – 495.

Table 1. Summary of sites drilled and cored during NGHP-01 (adapted from Table T1 of Collett et al., 2008). Question marks indicate uncertainty about sediment characteristics. "Combination" indicates that gas hydrate at this site was found both in sand/silt layers and in fractures. "Micro/Therm" indicates a mix of biogenic methane and thermogenic gas. Only sites for which in situ temperature measurements were made and a BSR was observed are included here.

Site	Water depth (m)	Depth to BGHS from downhole data	Depth to BGHS from seismic data	Dominant sediment type	Gas hydrate reservoir type	Gas source
NGHP-01-03	1076	203	209	Clay with silt/sand beds	Silt/Sand	Microbial
NGHP-01-05	945	130	~125	Clay with silt/sand beds	Combination	Microbial
NGHP-01-07	1285	198	188	Clay with silt/sand beds	Combination	Microbial
NGHP-01-10	1038	160	~160	Clay/silt	Fracture	Microbial
NGHP-01-14	895	116*	109	Clay with silt/sand beds	Silt/Sand	Microbial
NGHP-01-15	926	126	126	Clay with silt/sand beds	Silt/Sand	Microbial
NGHP-01-16	1253	178	170	Clay with silt/sand beds	Silt/Sand	Microbial
NGHP-01-17	1344	620	~608	Clay/silt with volcanic ash beds	Silt/Ash	Micro/Therm
NGHP-01-18	1374	210	~210	Clay/silt	Clay/silt?	Micro/Therm
NGHP-01-19	1422	220	205	Clay with silt/sand beds	Silt/Sand	Micro/Therm

*Note that the depth to stability boundary from downhole data for NGHP-01-14 is incorrect in the Initial Report (Collett et al., 2008) because of an incorrect predicted stability boundary. This error has been corrected in this table.

Table 2. Constants assumed for 1D models of the effect of sedimentation and erosion on apparent heat flow.

Constants assumed for 1D models of the effect of sedimentation and erosion	
Thermal conductivity of water	0.6 $Wm^{-1}K^{-1}$
Thermal conductivity of sediment grains	2.74 $Wm^{-1}K^{-1}$
Thermal conductivity of basement	2.9 $Wm^{-1}K^{-1}$
Thermal capacity of water	4.305×10^{6} $Jm^{-3}K^{-1}$
Thermal capacity of sediment	2.6×10^{6} $Jm^{-3}K^{-1}$
Thermal capacity of basement	3.3×10^{6} $Jm^{-3}K^{-1}$
Sediment heat generation	0.6×10^{-6} Wm^{-3}
Seafloor temperature	5.5°C at site 17

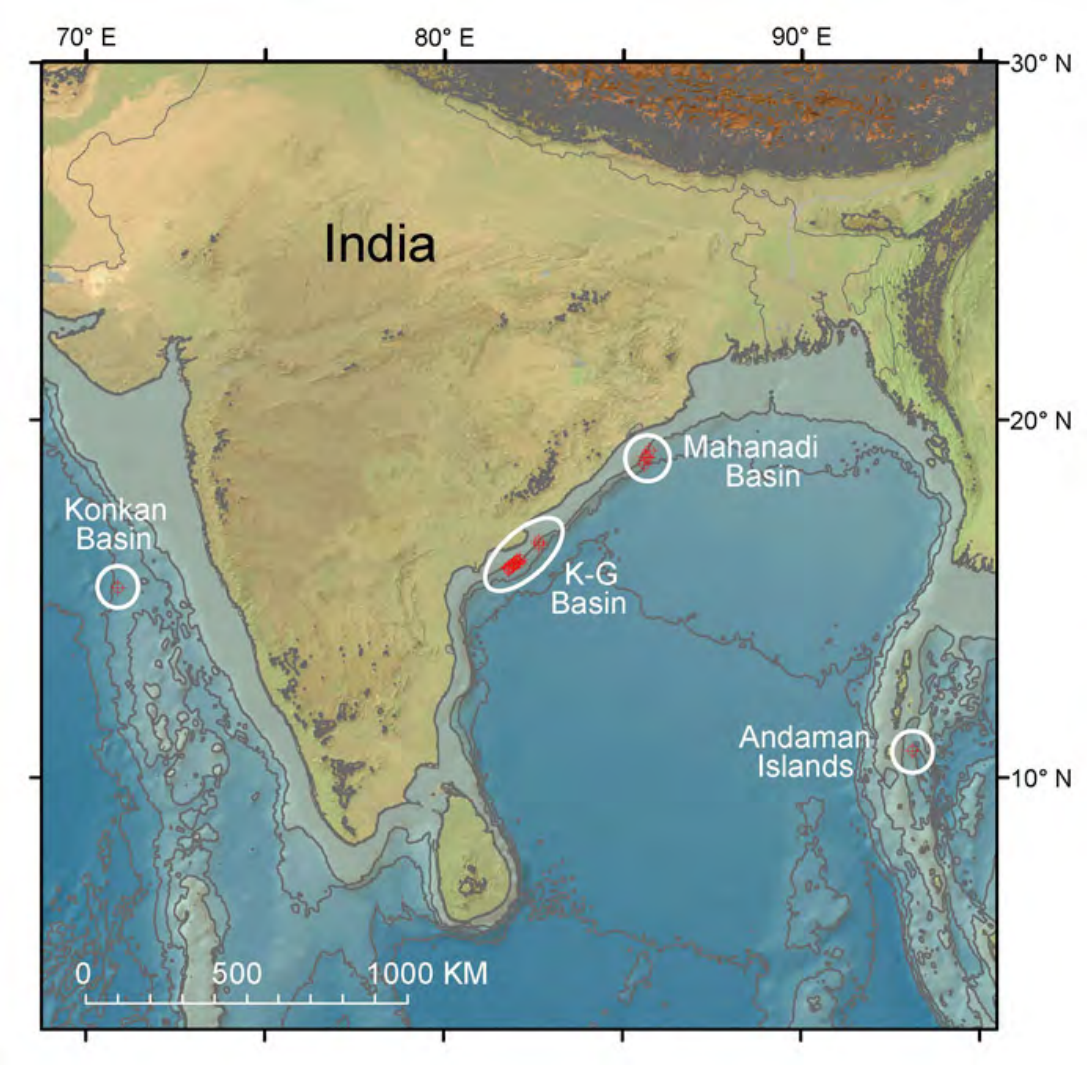

Figure 1A. Study locations from Indian National Gas Hydrate Program Expedition 01 (Collett et al. 2008). The three Bay of Bengal sites (Krishna-Godavari Basin, Mahanadi Basin, and Andaman Basin) are the focus of this study. The Konkan Basin site was not included because it lacks a BSR related to gas hydrate presence.

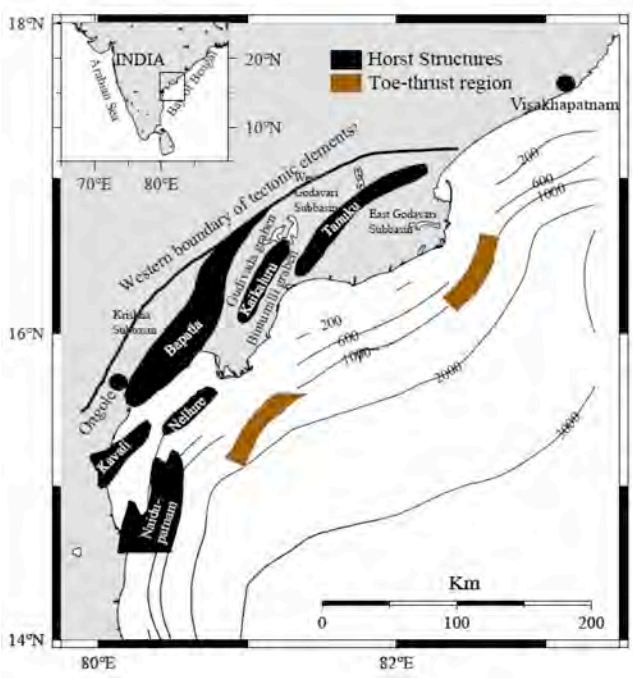

Figure 1B. Tectonic map of the K-G basin (from Dewangan et al., 2011). The continent/ocean boundary corresponds approximately to the 3000 m contour based on magnetic anomalies (Murthy et al., 1995).

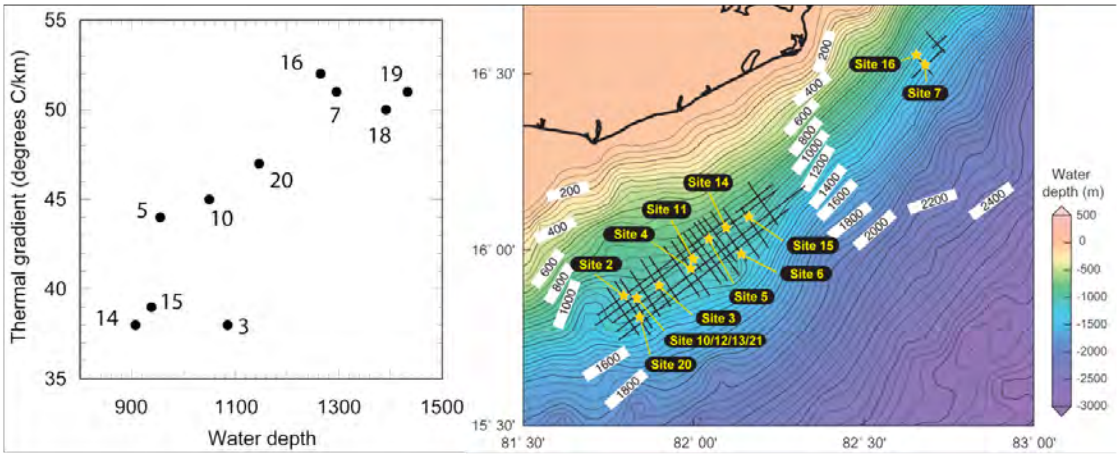

Figure 1C. (left) Thermal gradient from borehole observations versus water depth (Trehu, 2007). (right) Map showing location of boreholes in the K-G basin (from Collett et al., 2008). Sites 18 and 19 in (A) were located in the Mahanadi basin (see Fig. 1A).

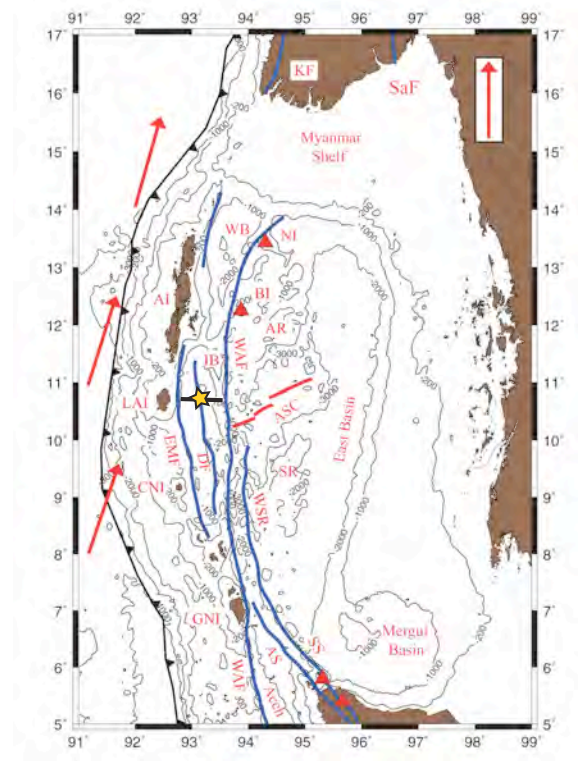

Site 17

WAF - West Andaman Fault
DF - Diligant Fault
EMF - Eastern Margin Fault
LAI - Little Andaman Island
ASC - Andaman Spreading Center

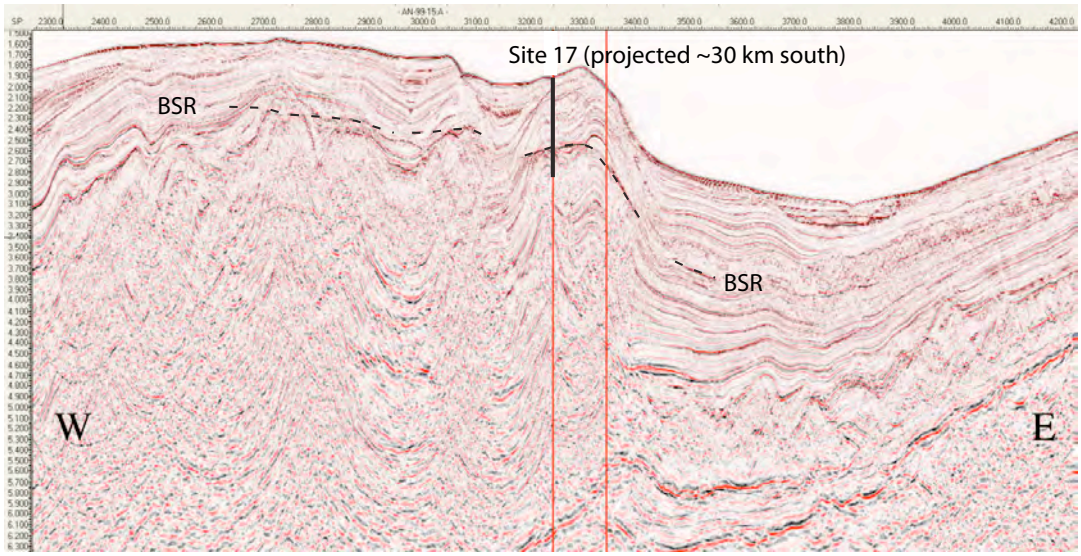

Figure 2. (A) Map of the Andaman Sea showing the location of Site 17 (from Cochran, 2010). Tectonic features near Site 17 and discussed in the text have been identified in the legend. For definitions of other abbreviations, see Cochran (2010; figure 1). Red triangles are volcanos. Red arrows show the plate vectors with the vector in the upper right corner showing a rate of 30 mm/yr. (B) Seismic line that extends approximately from the Eastern Margin Fault to the West Andaman Fault. Site 17 was located on the flank of a ridge corresponding to the Digilent Fault.

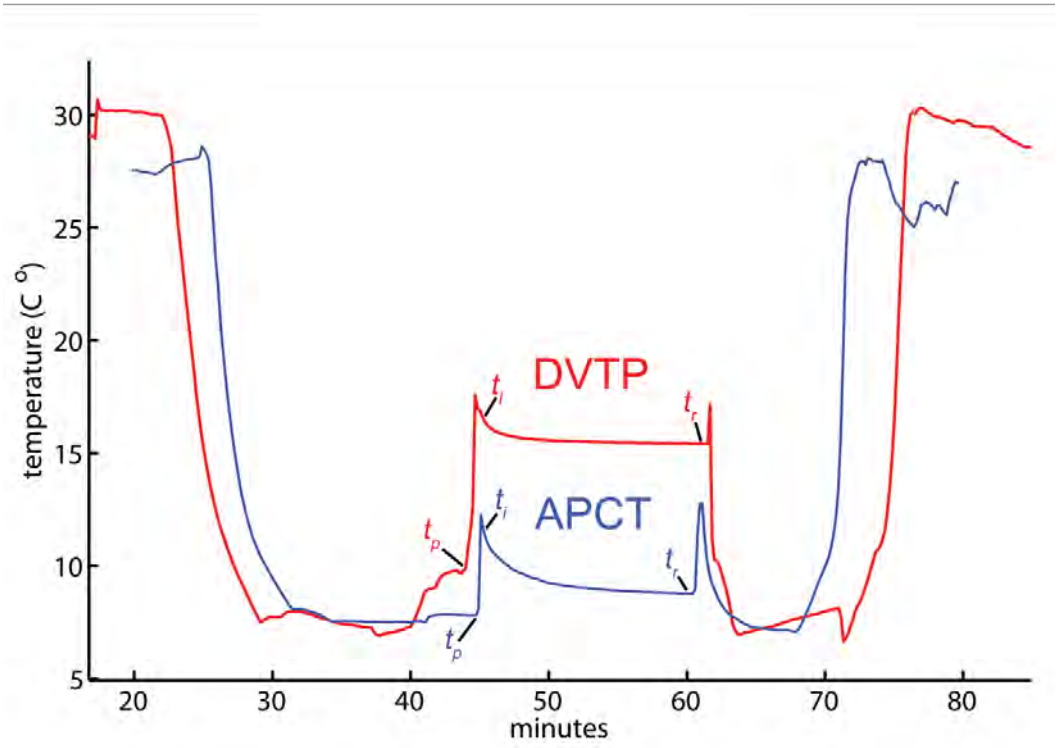

Figure 3A. Typical temperature tool runs. Advanced Piston Corer Temperature (APCT) tool run from NGHP Site 5 (blue) and the Davis-Villinger Temperature Probe (DVTP) run at site 10 (red). After cooling during its decent through the water column, the tool measures bottom water temperature followed by temperature in the borehole. The tool is then inserted abruptly into the sediment at the base of the borehole, causing a frictional pulse (t_p). The frictional heat pulse decays and another frictional spike is observed at the probe is recovered, indicating good coupling to the sediment. The window of data used to constrain the extrapolation to estimate in situ temperature is indicated by (t_i) and (t_r).

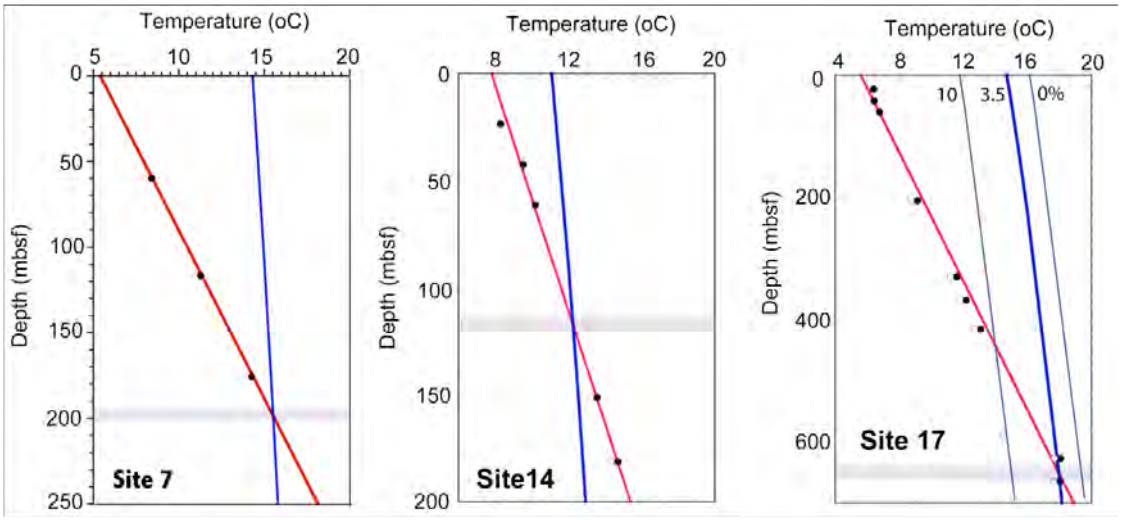

Figure 3B. Examples of temperature measurements made downhole at 3 NGHP-01 sites. See Collett et al. (2008) for all data. Filled circles are the uncorrected measurements and open circles are the same measurements after calibration corrections for different instruments, which were determined by submerging all instruments simultaneously in an ice water bath for several hours (Collett et al., 2008). If only open circles are visible, it is because the correction was to small to be apparent on this scale and the open circles cover the closed circles. The red line is the best-fit line through the points. The blue line is the methane hydrate stability boundary for seawater salinity. The plot for Site 17 shows the effect of salinity on the predicted stability boundary. The horizontal grey band is the range of predicted depths to the gas hydrate stability boundary. All NGHP-01sites had pore water salinities near the BSR that were between 3% and 3.5%.

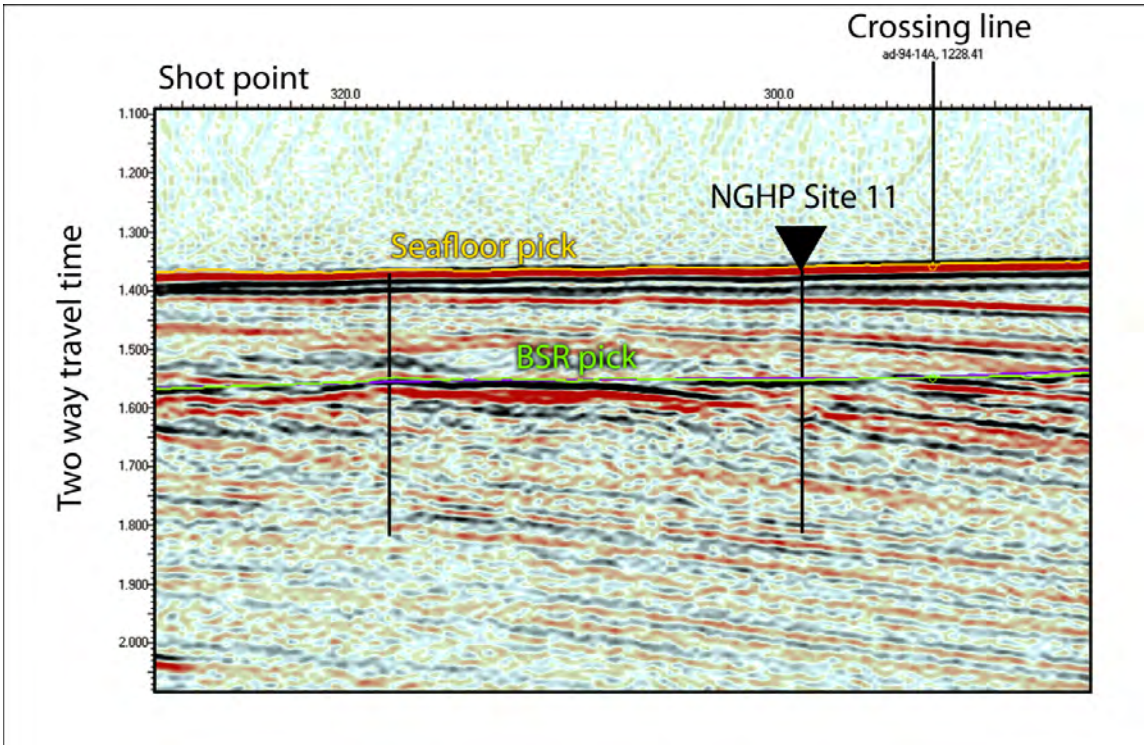

Figure 4. Example of a seismic line from K-G basin through site 11. The green line tracing the BSR shows BSR picks, and the purple line following it is the gridded interpolation produced by the Kingdom Suite seismic interpretation software. The yellow line is the seafloor pick. Open green and yellow circles on the BSR and seafloor pick lines indicate intersection points on crossing lines

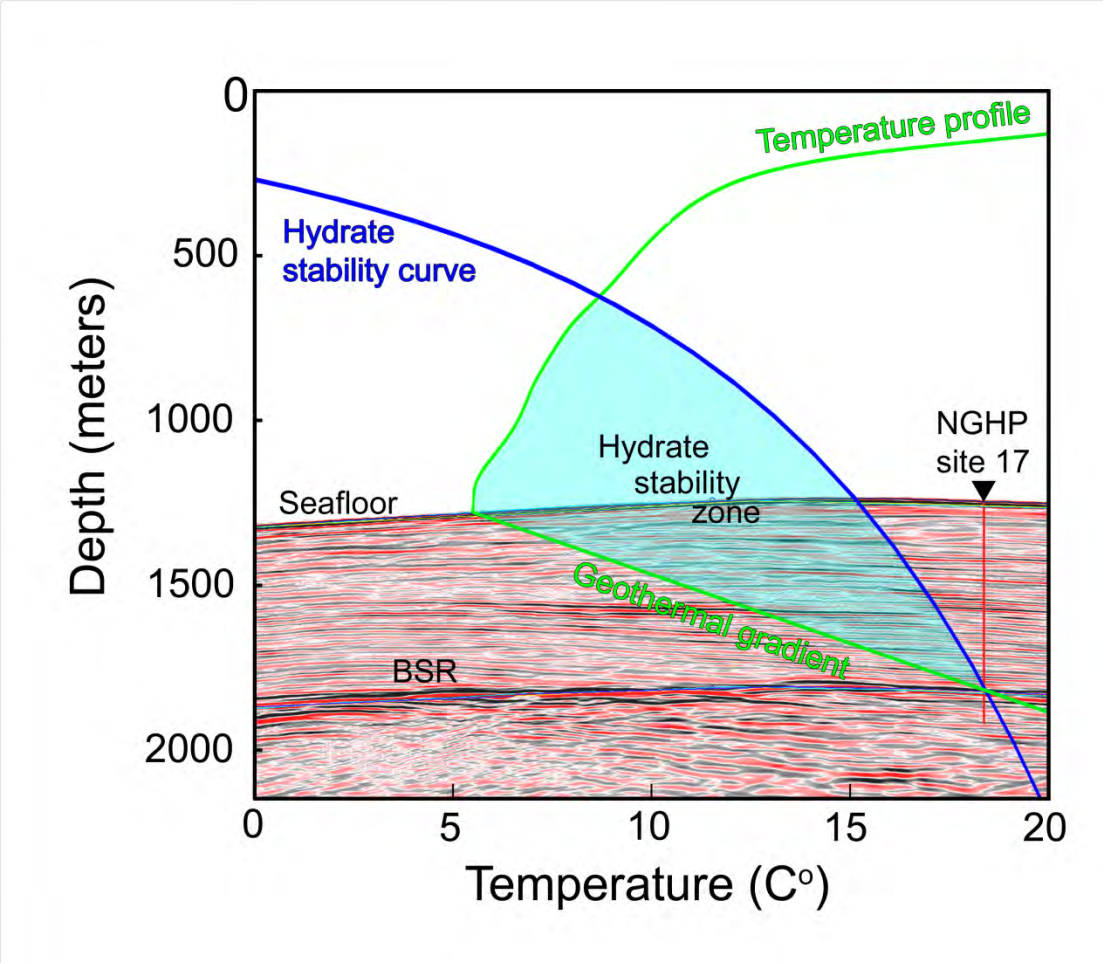

Figure 5. Hydrate stability curve assuming pure methane and 3.5% seawater calculated using CSMHYD (Sloan and Koh 2009) at NGHP site 17, in the Andaman Basin (blue line). The green line is the temperature profile for the Andaman Sea, with ocean temperatures from the World Ocean Atlas 2005 (Locarrini et al. 2005) and the geothermal gradient determined from NGHP site 17 downhole temperature measurements (Collett, et al. 2008). The seismic section shows a clear BSR at 1800 mbsl (608 mbsf).

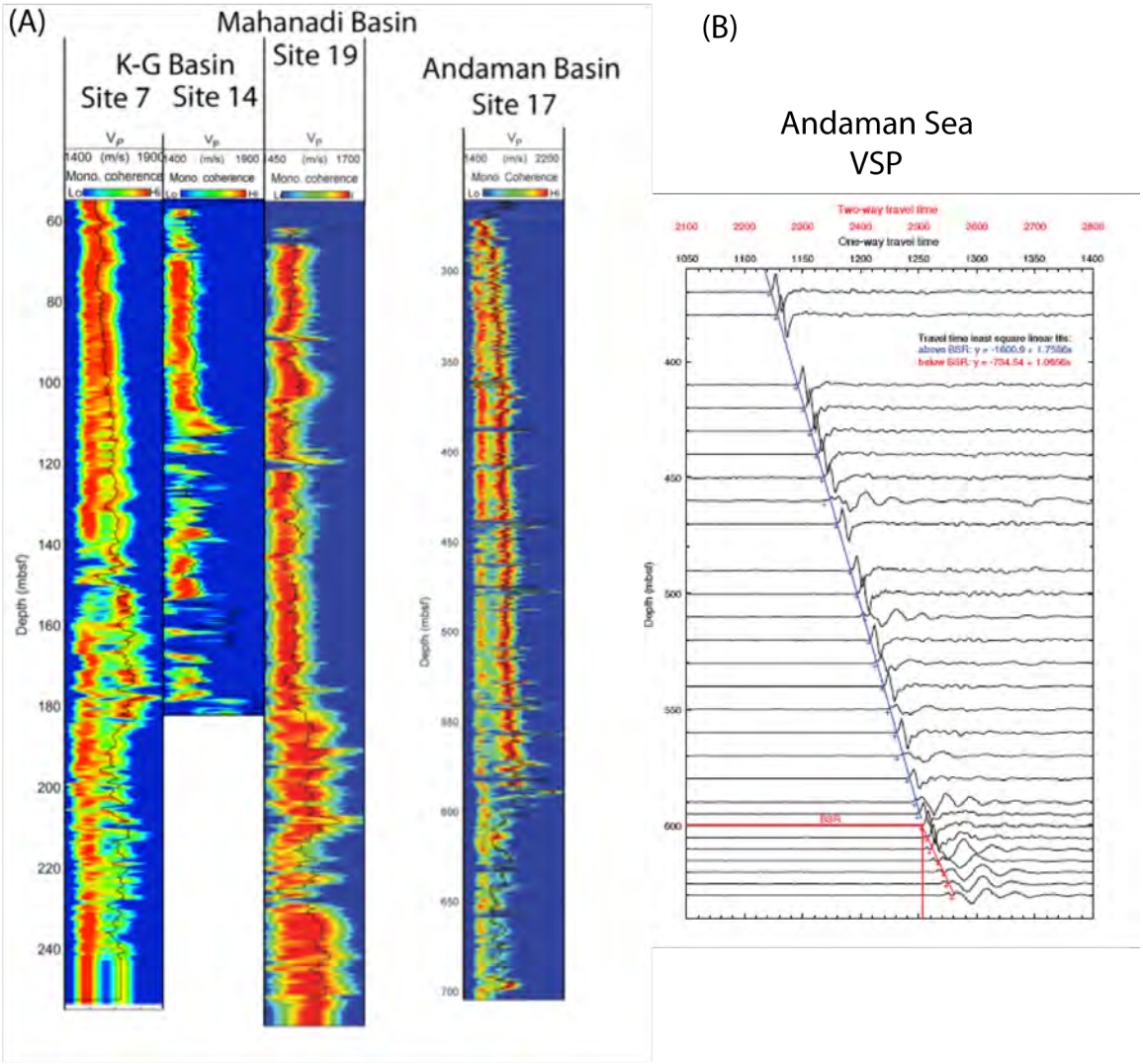

Figure 6. (A) P-wave velocity logs from the three study regions. For the K-G Basin, Mahanadi Basin, and Andaman Basin, average sediment p-wave velocities of 1550 m/s, 1550m/s and 1600 m/s, respectively were used for all calculations (from Collett et al. 2008). Note that although the log for Site 17 shows velocity increasing from 1600 to 1800 m/s from 300-600 mbsf, the velocity above 300 mbsf is likely below 1600 m/s. (B) Data from a vertical seismic profile conducted at Site 17, which shows an average velocity of 1601 m/s above the BSR. Uncertainty in sediment velocity is estimated to contribute ~2% to the uncertainty in the heat flow estimate through its effect on BSR depth and consequently pressure.

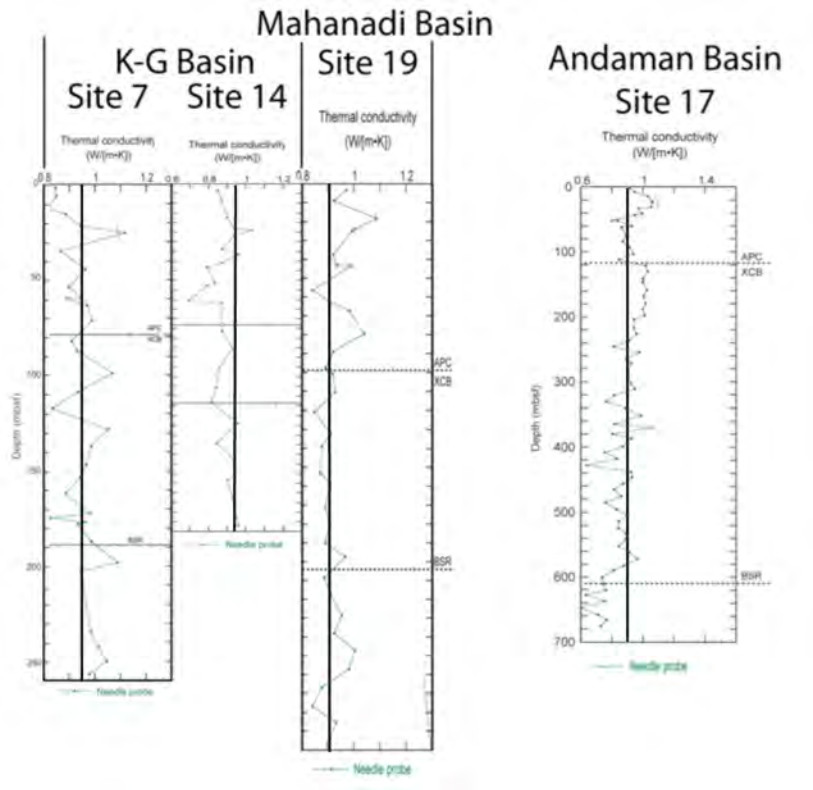

Figure 7. Thermal conductivities from shipboard measurements in representative wells from the three study areas (from Collett et al. 2008). Thermal conductivities used were 0.95 $Wm^{-1}K^{-1}$, 0.90 $Wm^{-1}K^{-1}$ and 0.90 $Wm^{-1}K^{-1}$ for the K-G basin, Mahanadi basin, and Andaman basin, respectively. The uncertainty in thermal conductivity is estimated to be ~0.05 $Wm^{-1}K^{-1}$, leading to an uncertainty of ~5% in estimated heat flow.

A

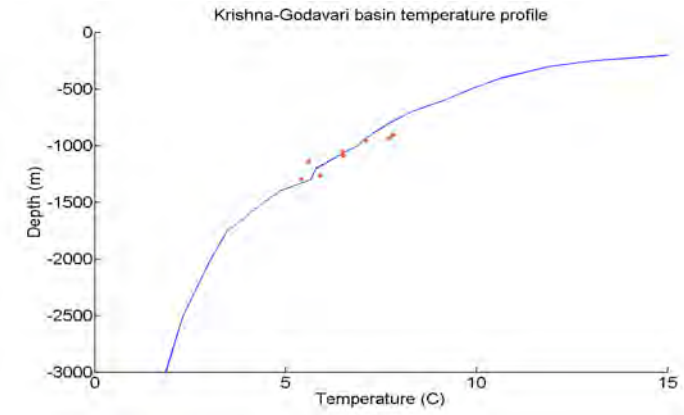

B

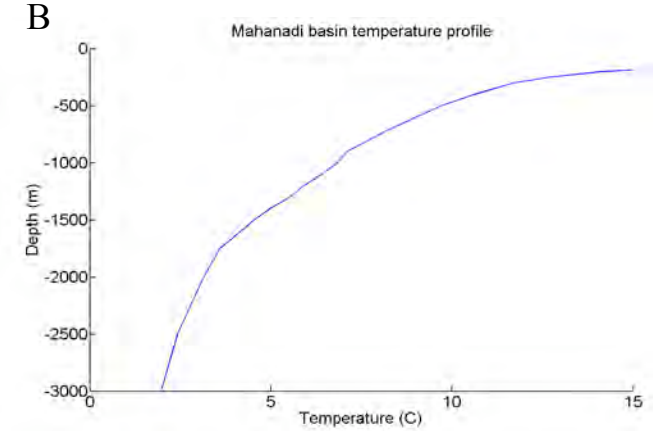

C

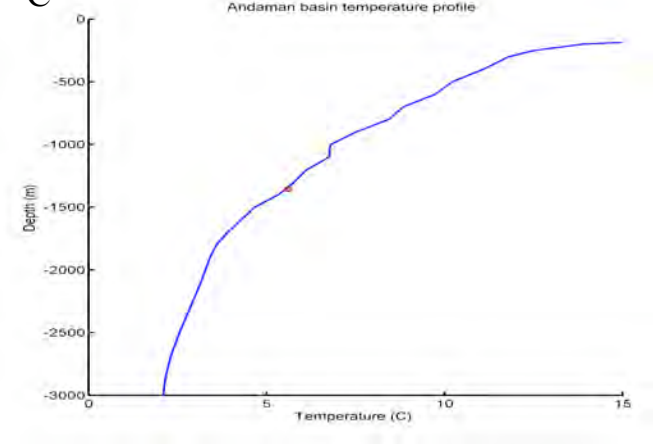

Figure 8. (A) Ocean temperature profile for the K-G basin. (B) Ocean temperature profile for the Mahanadi basin. (C) Ocean temperature profile for the Andaman Basin. Blue lines are from World Ocean Altas (Locarrini et al. 2005). Red points are bottom water temperatures derived from the downhole temperature tool.

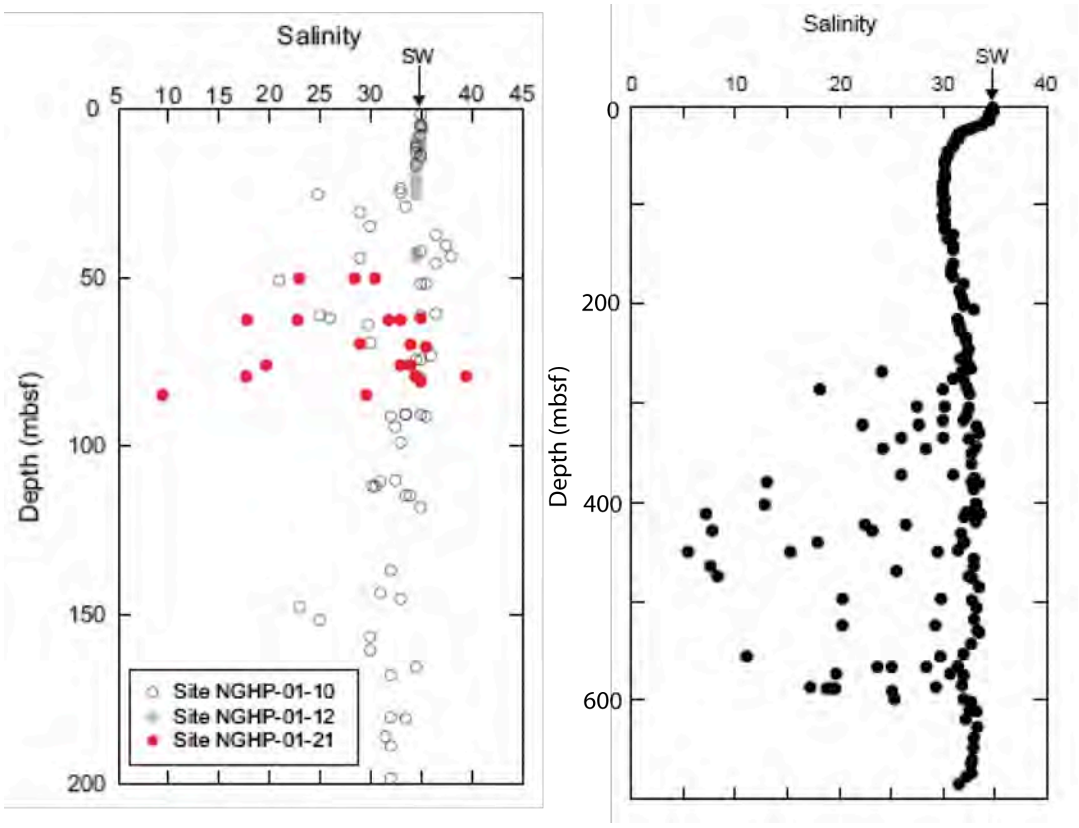

Figure 9. Porewater salinities from shipboard measurements in representative wells from the three study areas (from Collett et al., 2008). Anomalously low salinities are interpreted to represent porewater freshening when gas hydrate dissociated during core recovery. The background porewater salinity at all sites is in the range of 3.0-3.5%. Assuming a seawater salinity (3.5%) when calculating the temperature at the BSR results in an uncertainty of ~1% in estimated heat flow.

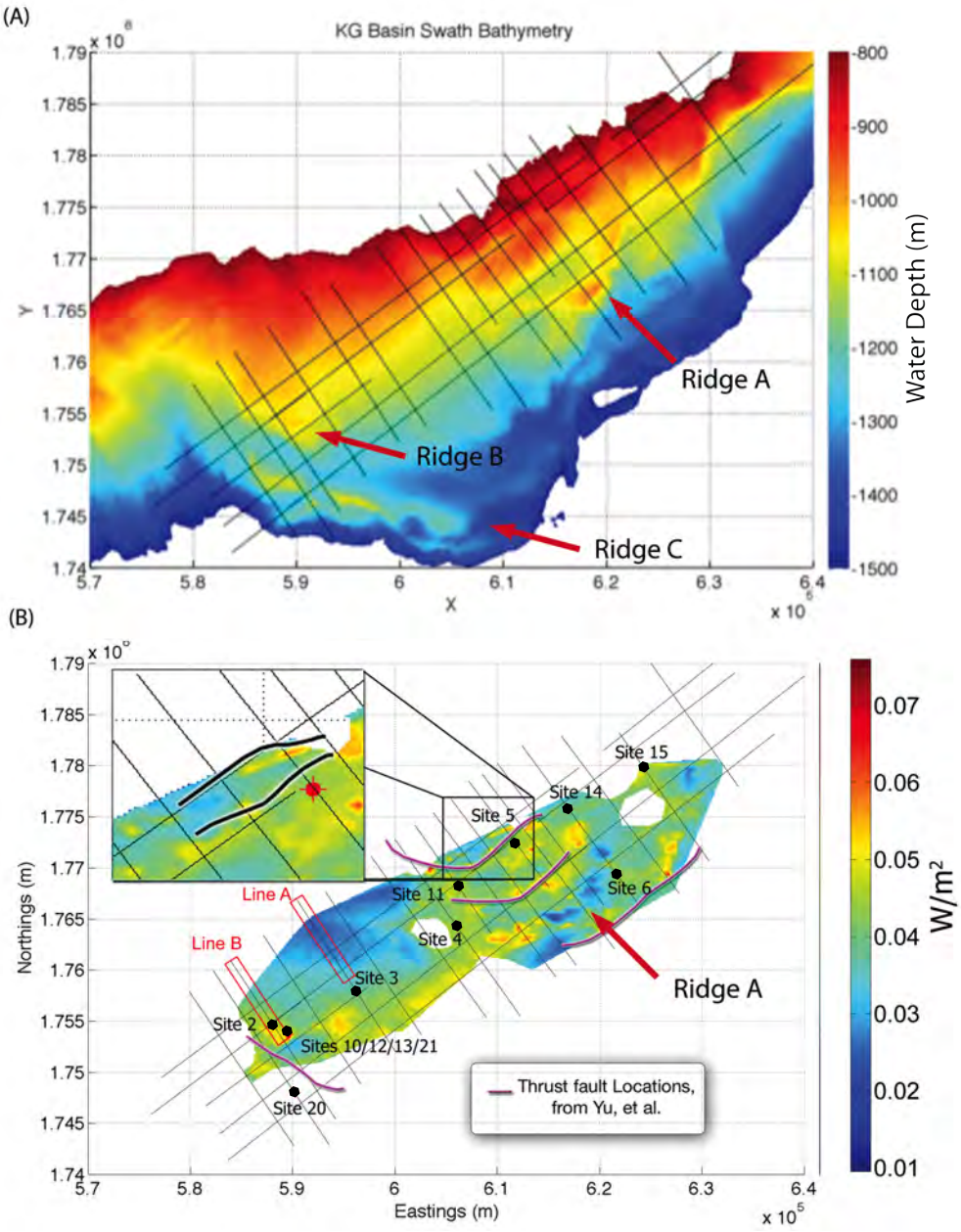

Figure 10. (A) K-G basin swath bathymetry, from 800-1500 meters water depth. Depths outside this depth window are not shown. Seismic survey lines are overlain in black. Bathymetry from 200-2200 m depth and many examples of the seismic lines are given by Shankar and Riedel (2010). (B) K-G basin apparent heat flow. Seismic survey overlain as black lines. Black hexagons represent NGHP Expedition 01 drill sites. Magenta lines are seafloor traces of faults, as found by Yu et al. (unpublished manuscript). Inset shows faults (black lines) identified by Yu et al. (unpublished manuscript).

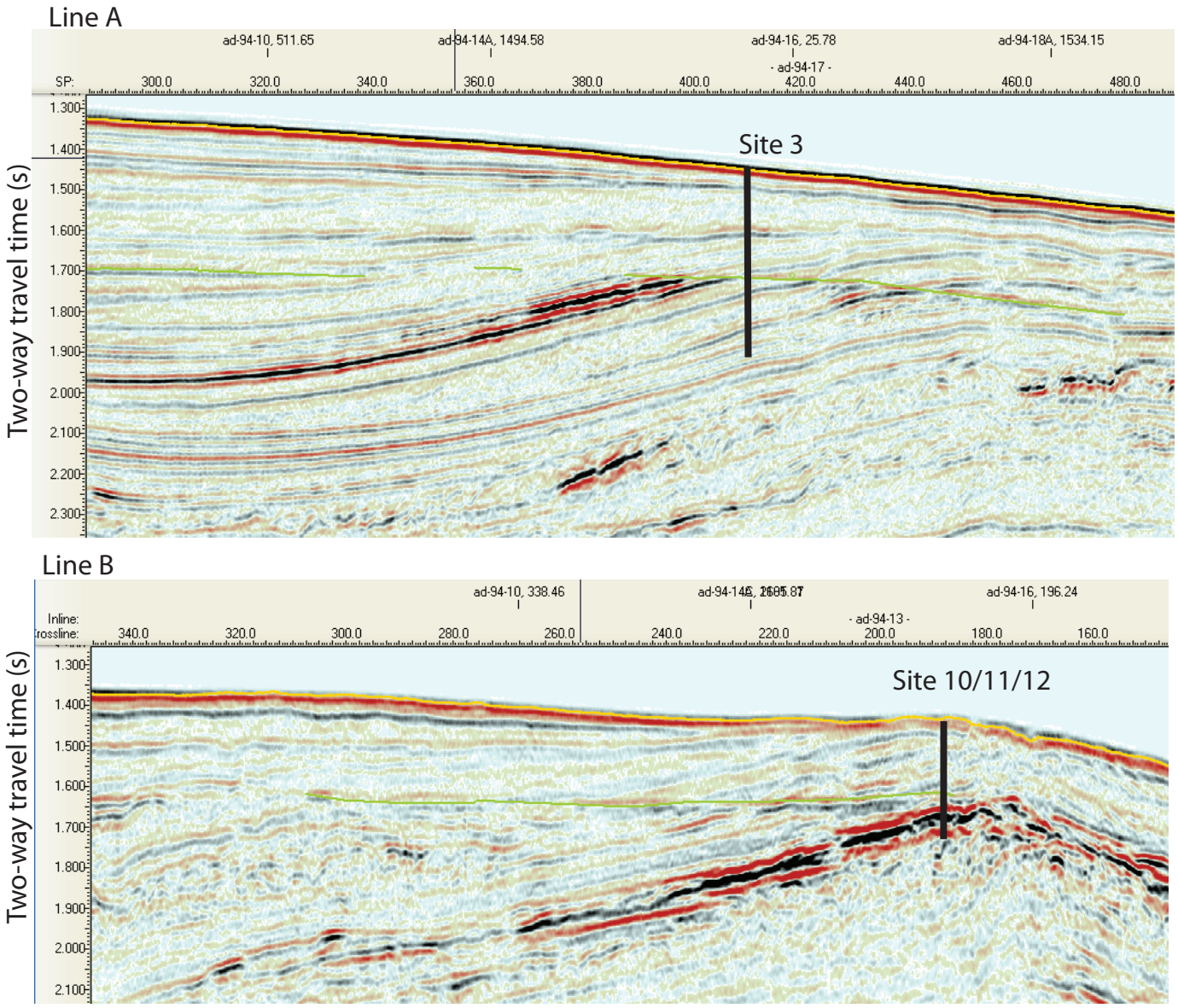

Figure 10. (C) Seismic sections showing the stratigraphic and structural setting of drilling sites 3 and 10. Orange line is picked seafloor reflection; yellow line is the BSR. On line 3, the BSR appears as a change in the reflectivity of dipping horizons. Both lines show patchy bright spots indicative of pockets of gas beneath the BSR.

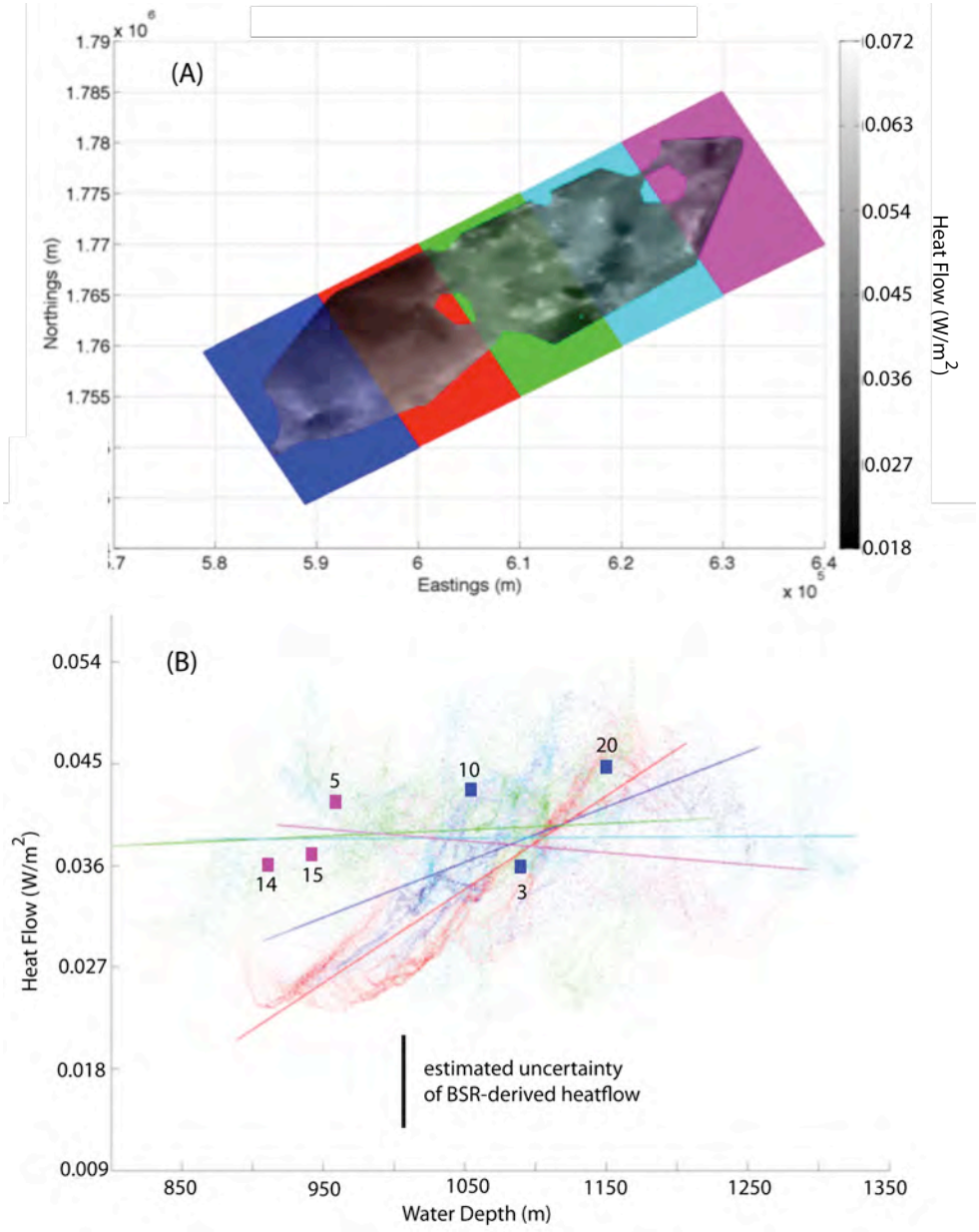

Figure 11. (A) Apparent heat flow map of the K-G basin, with five zones shown overlain in various colors. (B) Cloud plot showing variation of apparent heat flow as a function of depth. The color of the data points and best fit lines are color-coded to the regions in (A). In the blue and red regions, apparent heat flow increases with increasing water depth, which we attribute to formation of a slope basin behind a toe-thrust (see text). In the green, cyan and magenta regions, local apparent heat flow variations are controlled by local features and no systematic regional trend is resolved.

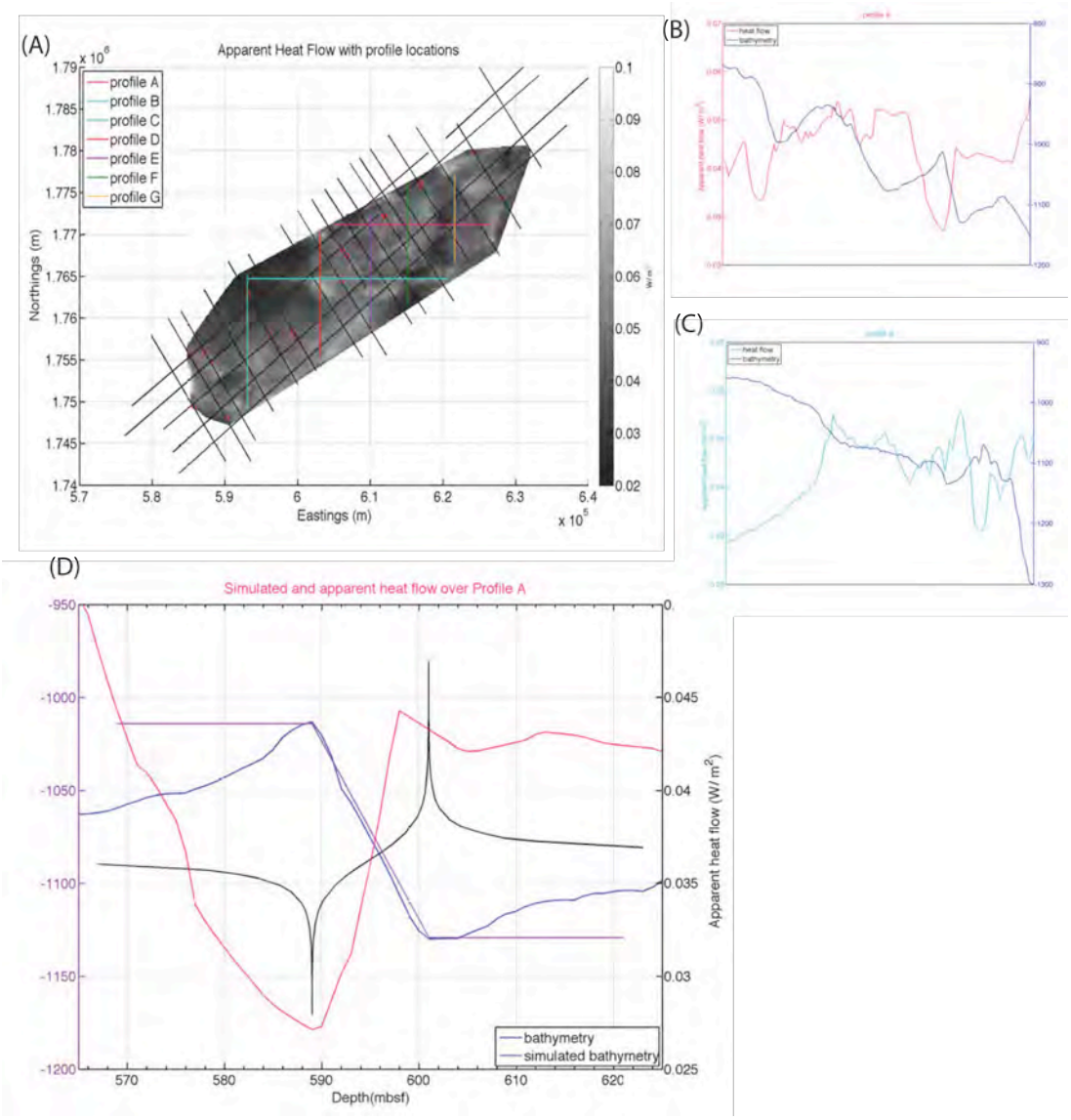

Figure 12 (A) Map of BSR-derived heat flow showing location of seismic lines (black) and lines selected to show correlations between topography and heat flow. See Figure 11A for the scale for the heat flow map. Only profiles A and B are shown here; the others are shown in the technical report for the 3rd quarter of this project. (B) Heat flow and topography along profile A. Note the clear inverse correlation between the ridge on the eastern end of this profile and a pronounced trough in the heat flow. (C) Heat flow and topography along profile B. The correlation between the topographic ridge and heatflow trough is also seen on this profile. In addition, there is a correlation between decreasing water depth and decreasing heat flow on the western end of this profile. This latter effect will be discussed in the section on 1D modeling of the effects of variable sedimentation rate. (D) Simple analytical model of the effect of topography on heat flow (Lachenbruch, 1989). In the future, we may build on this inital result by modeling the effect of topography in 3D using the method of Blackwell (1980) as implemented by Harris et al. (in press).

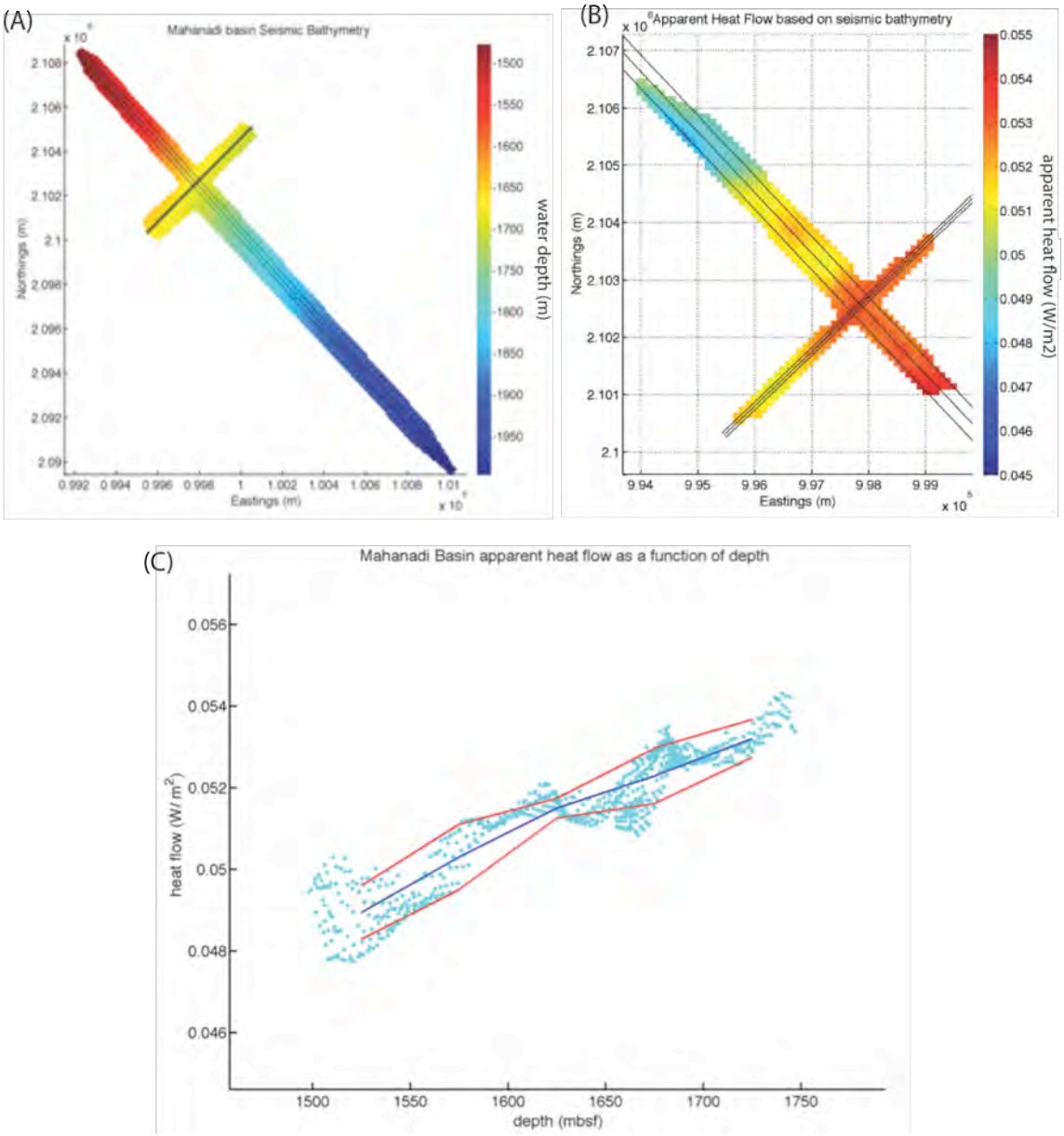

Figure 13. (A) Mahanadi Basin bathymetry based on seismic surveys (shown as black lines). (B) Mahanadi basin apparent heat flow map. (C) Apparent heat flow vs. water depth in the Mahanadi basin with best fit line (blue line) binned over 50 meter depth windows, bracketed by the standard deviation of bins (red lines). Although an apparent increase in heat flow with increasing water depth is observed, the total range of values represented is small and is within the total uncertainty of the accumulated uncertainties in thermal conductivity, seafloor floor temperature, pore water and gas chemistry and seismic velocity/density. We cannot rule out a systematic down-slope change in all of these parameters in such a way that is would produce this result even if actual heat flow were constant.

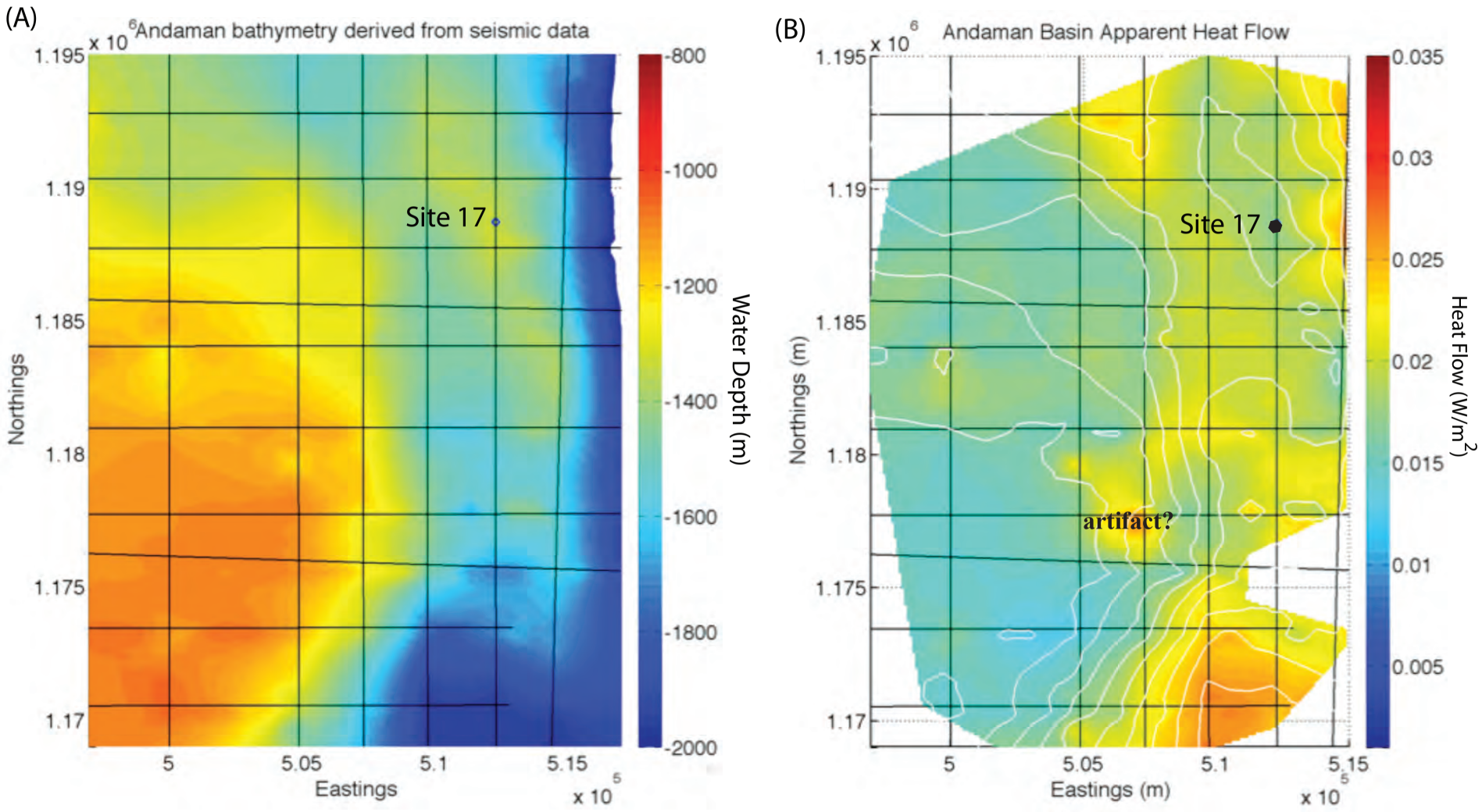

Figure 14. (A) Andaman Sea bathymetry. Blue circle in the northeast portion of the map represents NGHP site 17. Andaman pre-cruise seismic survey grid is overlain in black. (B) Apparent heat flow in the Andaman Basin. The blue circle is site 17 from NHGP-01. Black lines represent seismic survey lines. White lines indicate seafloor bathymetry.

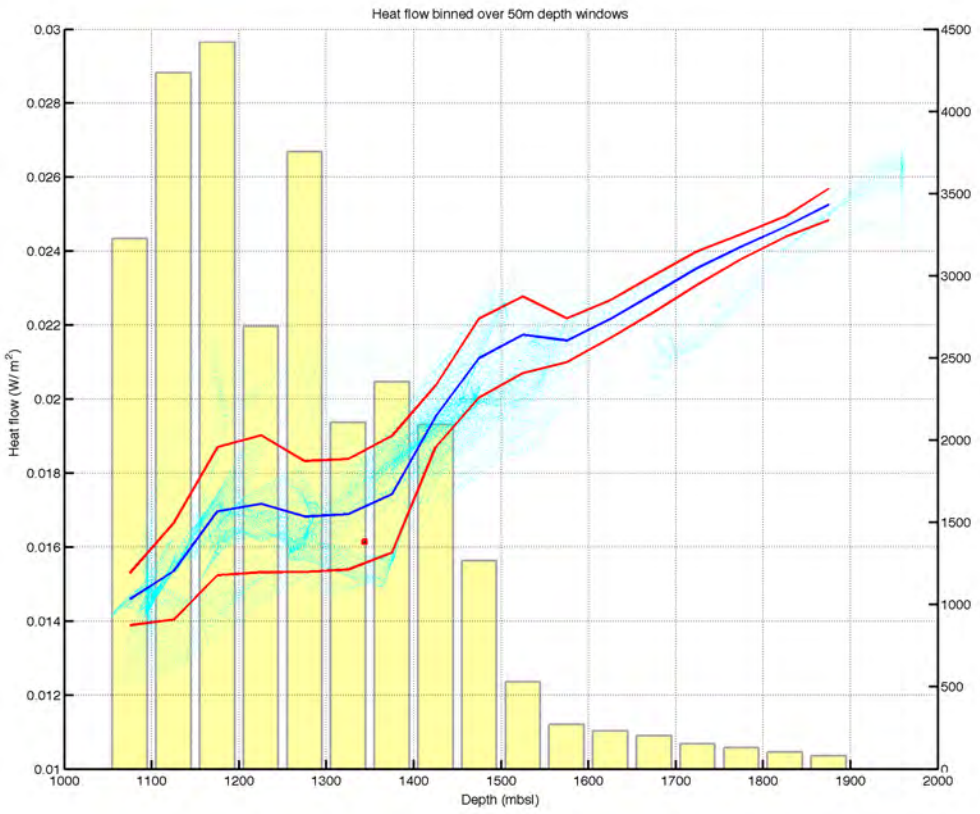

Figure 15. Heat flow as a function of depth for the Andaman Basin (cyan points). Overlain are average apparent heat flow values binned over 50m depth windows (blue line) showing one standard deviation (red lines). Borehole heat flow at site 17 shown as red open square. Light yellow bar graph represents the sample count for each depth bin

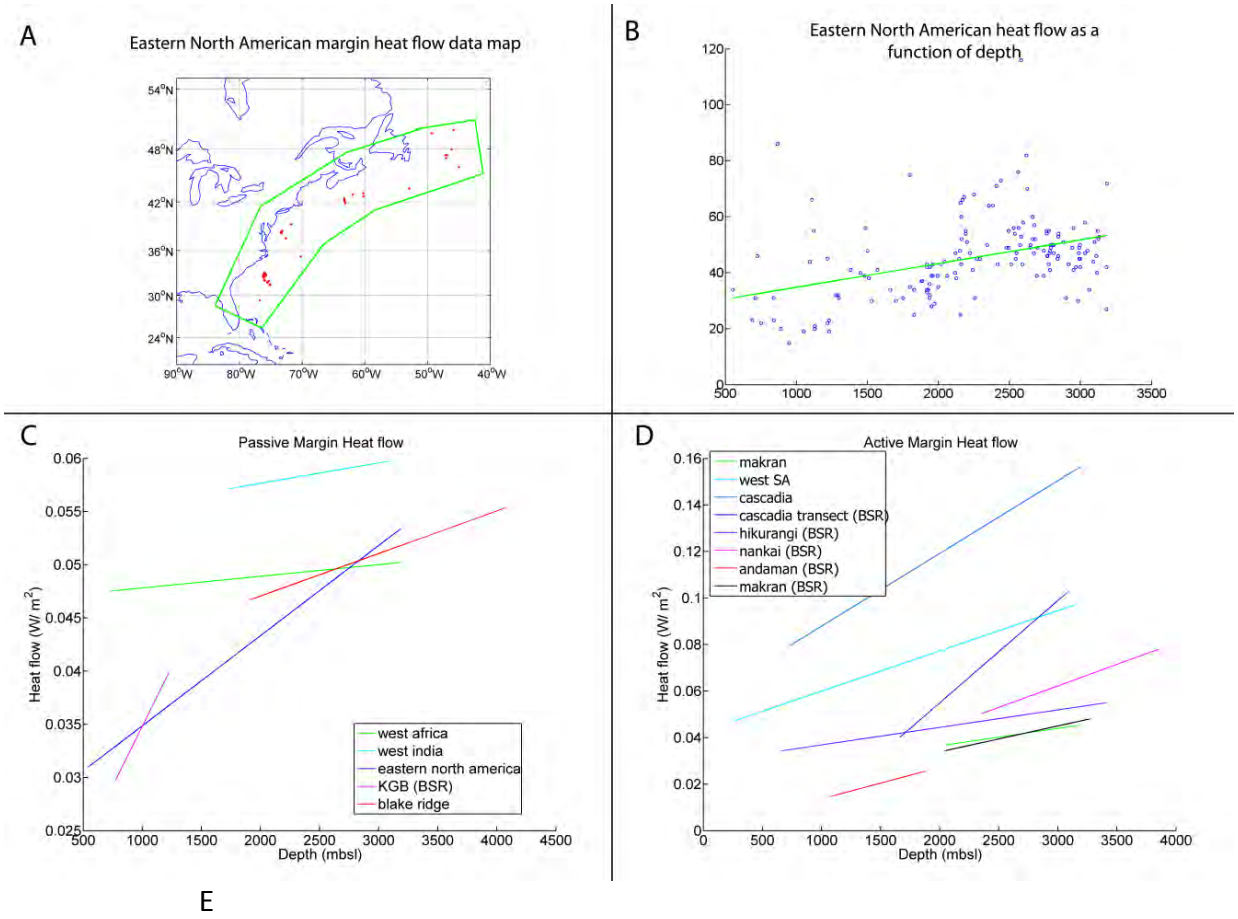

Figure 16. Heat flow compiled from many hydrate-bearing continental margins and from ocean basins. (A) Example of using the Global Heat Flow Database (Hasterok 2010) to obtain data from eastern North America. Red points show locations of heat flow samples that fall within the user-specified green box. (B) Eastern North American heat flow data (blue points) as a function of depth for data from (A). Best-fit line shown in green. (C) Best-fit lines to heat flow data from hydrate-bearing passive margins. Data from temperature probes unless noted as (BSR) in the legend. (D) Active margin heat flow compilation. Note different scales compared to C.

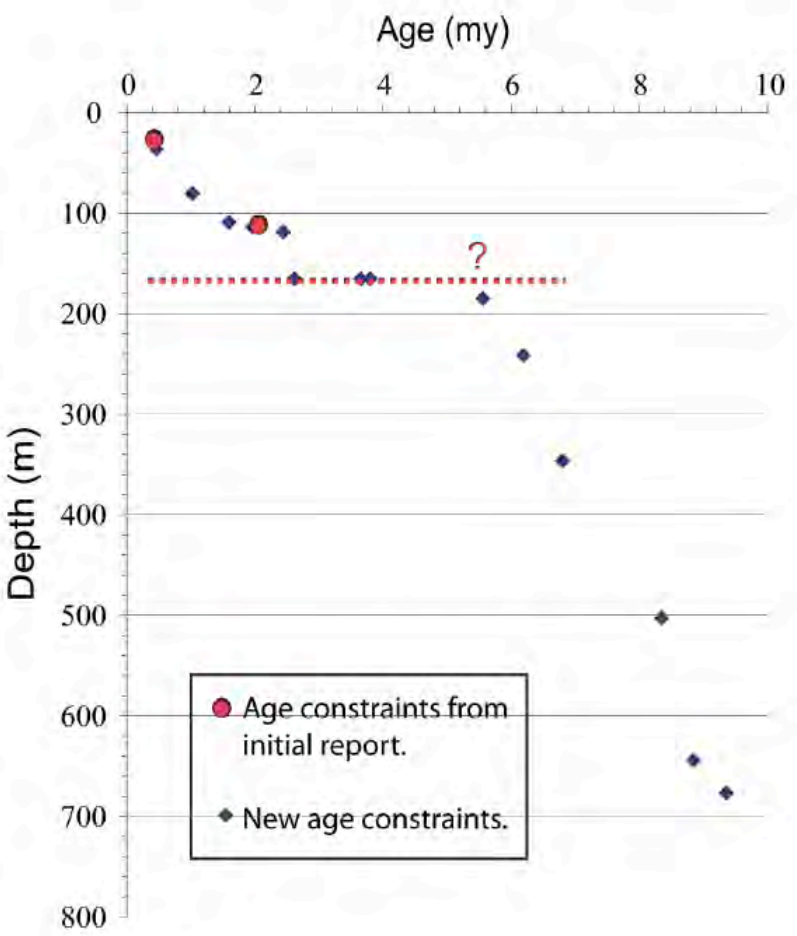

Figure 17. Updated age model showing age constraints from shipboard studies (Collet et al., 2008) and updated age constraints from Flores et al. (2008) and Cawthern et al. (2010). There appears to be an unconformity where the region experienced either an erosional or slow sedimentation period from 2.4 to 5.8 Ma.

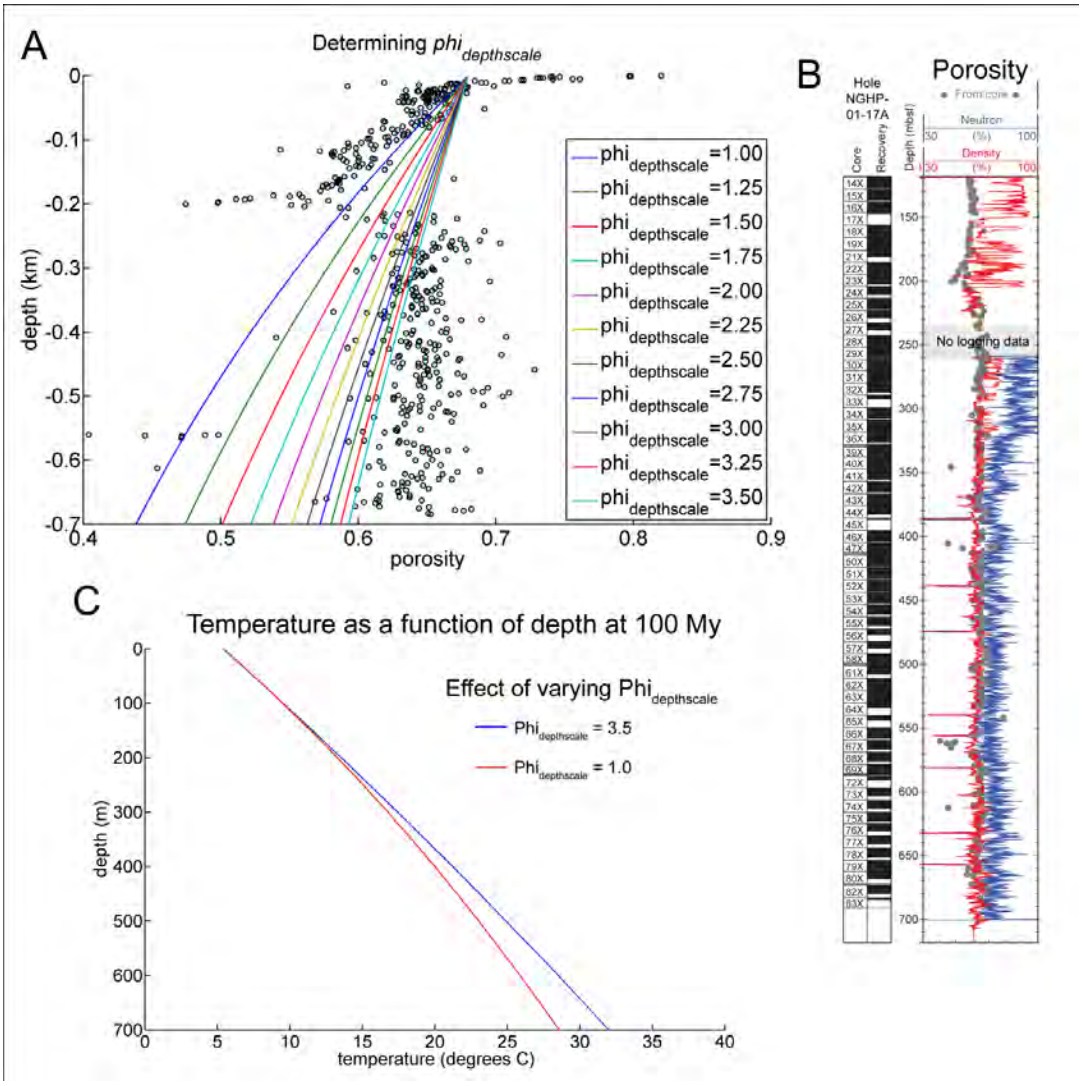

Figure 18. (A) Shipboard porosity measurements made from Site 17 core samples shown as green and black open circles. Note the abrupt change in porosity at 0.2 km depth. Multiple $phi_{depthscale}$ plots are given to show the sensitivity of the exponential depth-porosity relationship to this term. (B) Porosity measurement from downhole logging tools. Grey dots are shipboard measurements of porosity, plotted at the same scale as the logging data. Logging suggests consistently higher porosity than measurements on samples in the upper 300m of sediment, but trend similar to shipboard samples. (C) Modeled temperature gradient for the upper 700 mbsf after 100 My at 5.7 cm/ky sedimentation rate for two $phi_{depthscale}$ values, 1.0 and 3.5. A $phi_{depthscale}$ value of 3.5 was used in all models.

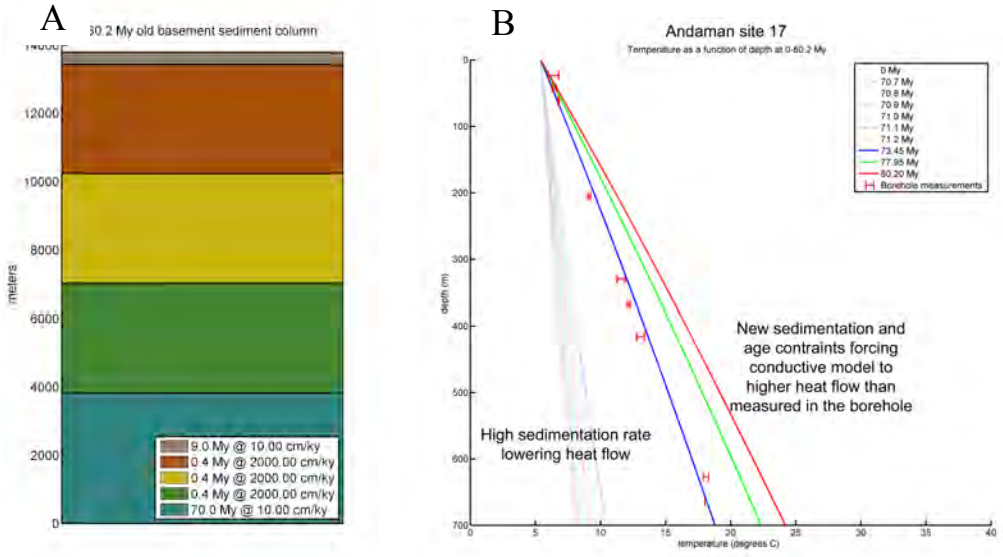

Figure 19. (A) Sedimentation history based on updated age constraints used to model conductive heat flow at NGHP site 17 in the Andaman Basin. Initial ship based age constraints truncated the most recent sedimentation period of 10cm/ky to only 2 My. Subsequent investigations found additional biostratigraphic datums which increased the time period characterized by this sedimentation rate to 10 My. (B) Temperature as a function of depth modeled for the last 10 My using age constraints from Figure 17. Times are in basement age. Time zero is initial formation, and 80.2 My corresponds to the present. Dotted lines indicate geothermal gradient at times of an assumed very high sedimentation rate (2000 cm/ky), which was estimated from the rate needed to match the data assuming sedimentation at 10 cm/ky for the last 2 MA (blue line), as indicated in the Initial Report (Collett et al., 2008). This is a simplified 1D way of incorporating tectonic thickening of the accretionary wedge followed by slope basin sedimentation. Green and red lines show the effect of increasing the time for slope basin sedimentation to correspond to the new biostratigraphic constraints. Error bars show temperature values and associated error measured using borehole temperature tools. The model shows very low and decreasing near-surface geothermal gradients throughout the high sedimentation rate period and increasing near-surface geothermal gradients during recent, lower sedimentation rate time. Expanding the amount of time during which sedimentation rate is constrained requires increasing the earlier sedimentation rate. This exercise shows how predicting heat flow in forearcs is complicated by the need to consider both the tectonic thickening and heat flow depression related to the accretionary wedge formation and slab deeping, and the forearc basin sedimentation that is simultaneously active during this process. The very low heat flow in the Andaman basin may reflect both a high rate of forearc thickening and a high rate of forearc basin sedimentation, compared to other forearcs, but data are not adequate to independently constrain these factors.

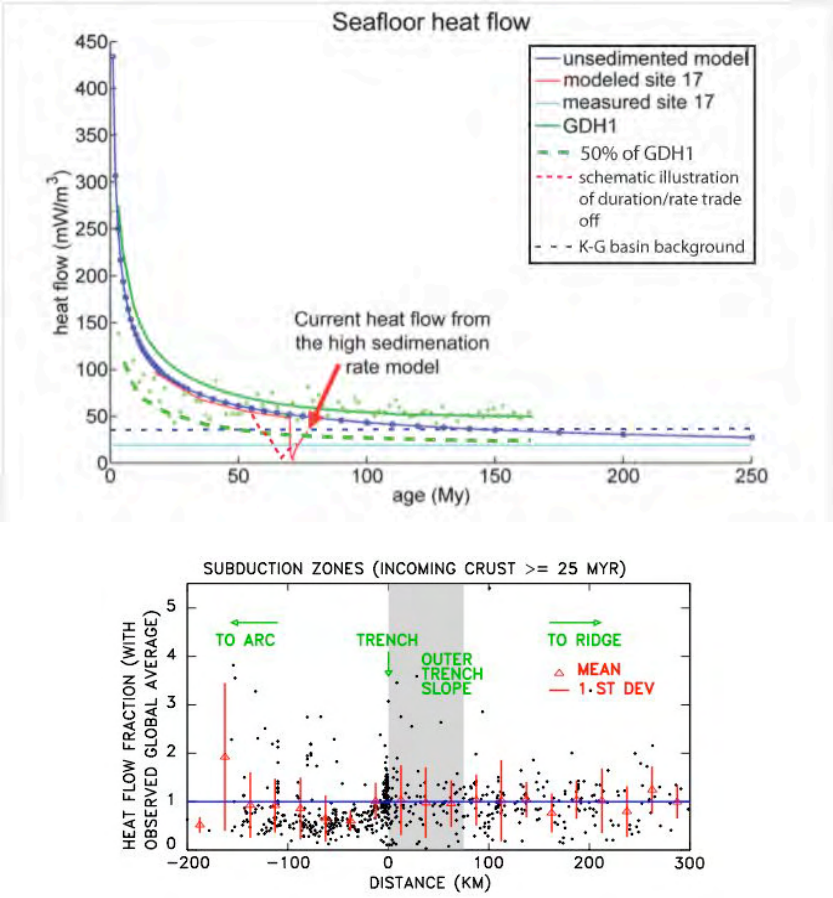

Figure 20. (top) Heat flow as a function of plate age. The blue line is an unsedimented 1/2-space model for the parameters we used for 1D modeling (Table 2). The green line is the GDH1 model (Stein and Stein, 1992); green dots are measured heat flow values. Dashed green line is 50% of GDH1, which is the heat flow generally seen in forearc basins (Stein, 2003). The horizontal cyan line shows the current measured apparent heat flow at Site 17, which is 33% of the GDH1 prediction and ~70% lower than the value expected in a forearc basin overlying 70-80 million year old subducted plate. The red line is the apparent seafloor heat flow as a function of plate age modeled using age constraints from Site 17 (see Figure 19). The sharp drop in apparent heat flow is from an increase in sedimentation rate, and the following rise is a result of changing the sedimentation rate to values based on the biostratigraphic data. The dashed red line schematically shows the trade-off between the duration of time of very rapid sedimentation and the sedimentation rate during this time period. Including such an episode in the model is an ad-hoc way of incorporating the effect of tectonic wedge thickening in a 1D model and without a longer sedimentation and tectonic history the duration and rate are very poorly constrained. The dashed blue line is the average background heat flow in the K-G basin excluding the effect of sediment piling up behind a toe-thrust in the SW part of the study area, and shows that it is similar to the heat flow expected for the age of initiation of seafloor spreading in this region. (bottom) Global heat flow compilation for subduction zones, normalized to the expected heat flow for the GDH1 model and plotted versus distance from the deformation front (from Stein, 2003).

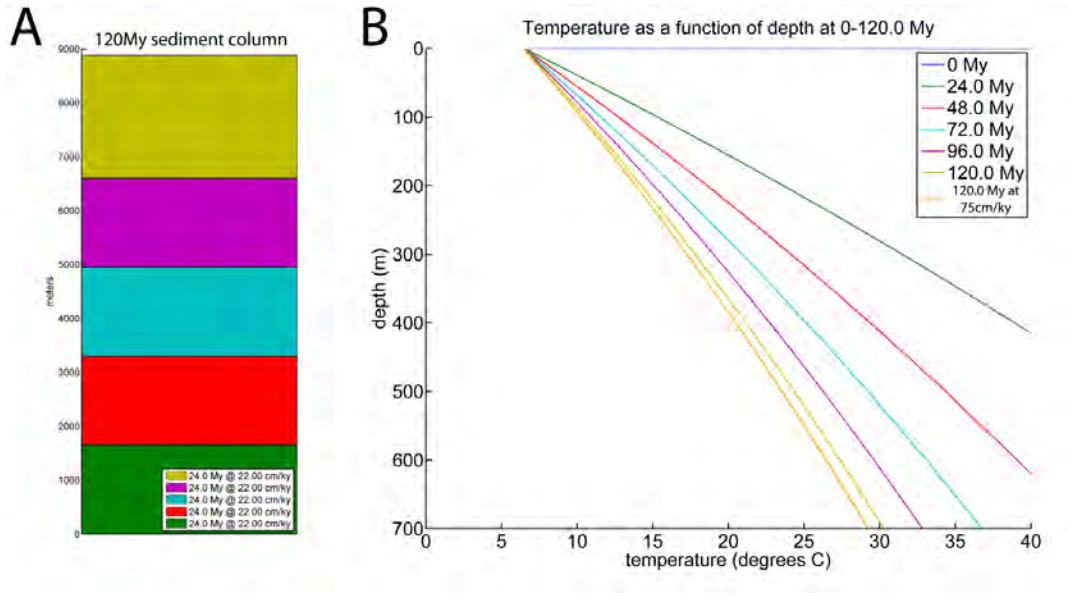

Figure 20. (A) Sediment column modeled for the K-G Basin. Assumed sedimentation rate of 22 cm/ky over 120 My in 24 My increments. (B) Temperature as a function of depth in 24 My time steps in the K-G Basin. Light orange line indicates the impact on the geothermal gradient of increasing the sedimentation rate to 75 cm/ky for the last 1.1 My. This increased sedimentation rate depresses the apparent geothermal gradient by ~10%, providing ~1/2 of the decrease needed to explain the observations relative to the background heat flow of 40 mW/m^2. The additional depression in heat flow may come from either a decrease in thermal conductivity or lateral convective heat transport, or some combination thereof.

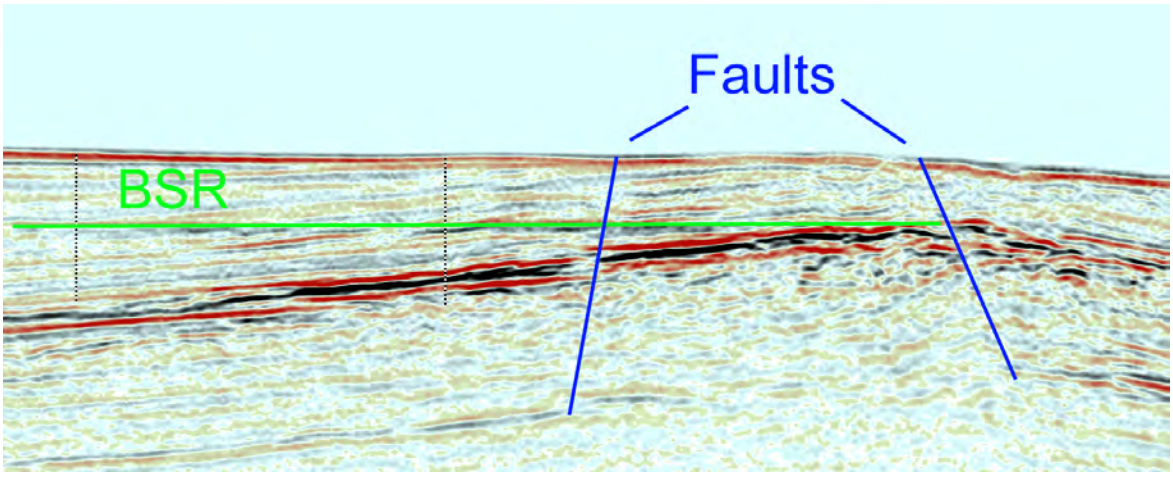

Figure 21. Detail from line B in Figure 10C showing potential advective transport pathways. Subhorizontal bedding leads to faults down slope from the ridge crest. This ridge crest was the site of the highest concentrations of methane hydrate found during NGHP Expedition 1. Green line crosscutting the bedding planes is the BSR. Faults are indicated by sub-vertical blue lines.

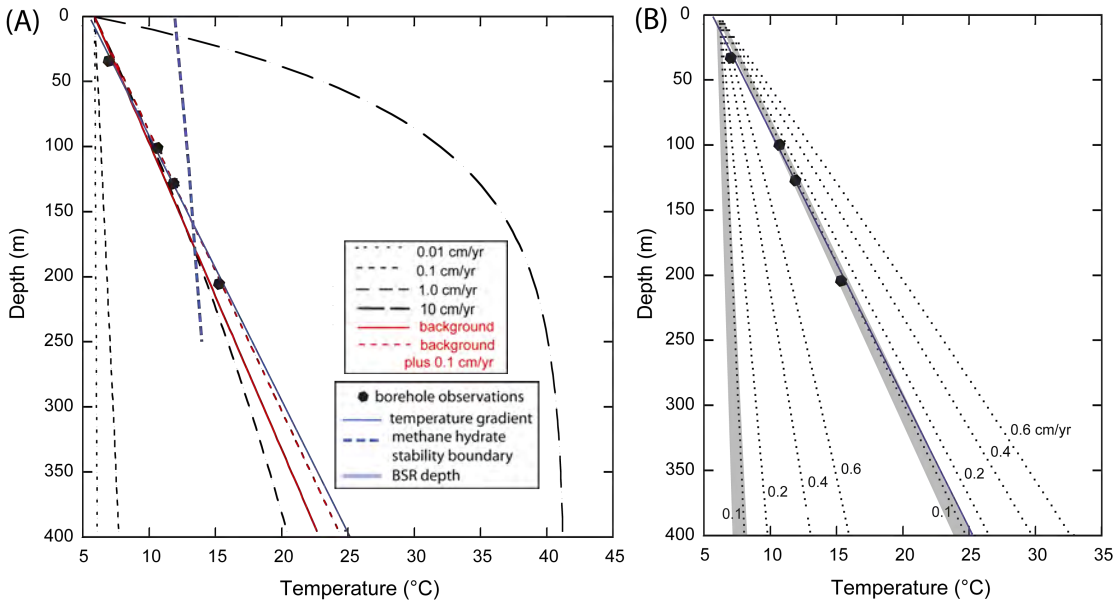

Figure 22. (A) Effect of upward heat advection on the temperature profile from a 1D model (Turcotte and Schubert, 2002). Calculations are shown for advection only for upward flow velocities of 0.01- 10 cm/yr (black dashed lines for a reservoir at depth at 42 degrees and the vertical flow rates shown in the legend) and for advection at 0.1 cm/yr added to the background regional gradient of 0.042°C/m (red lines). Values assumed for the thermal properties of the fluid and sediment are given in the text. The in situ temperature data for Site 10, the best-fit temperature gradient, the methane hydrate stability boundary and the BSR depths are also shown. A flow rate of 0.1 cm/yr added to the regional temperature gradient fits the data well. (B) Predicted thermal gradients for flow rates of 0.1-0.6 cm/yr, with and without a background temperature gradient (dotted lines) and the sensitivity of the temperature gradient to uncertainty in the thermal properties of the fluid and sediment. The shaded area shows the range of thermal gradients obtained for thermal sediment thermal conductivity of 0.9-1.0 W/(mK) and a range of specific heats for the fluid of 2.50-4.185 x 10^3 J/(kgK). An estimate of flow rate of ~0.1 cm/yr is indicated.

National Energy Technology Laboratory

626 Cochrans Mill Road
P.O. Box 10940
Pittsburgh, PA 15236-0940

3610 Collins Ferry Road
P.O. Box 880
Morgantown, WV 26507-0880

One West Third Street, Suite 1400
Tulsa, OK 74103-3519

1450 Queen Avenue SW
Albany, OR 97321-2198

2175 University Ave. South
Suite 201
Fairbanks, AK 99709

Visit the NETL website at:
www.netl.doe.gov

Customer Service:
1-800-553-7681